

A Study of the Type Ia/IIn Supernova 2005gj from X-ray to the Infrared: Paper I ^{1,2,3,4}

J. L. Prieto⁵, P. M. Garnavich⁶, M. M. Phillips⁷, D. L. DePoy⁵, J. Parrent⁸, D. Pooley^{9,10},
V. V. Dwarkadas¹¹, E. Baron^{8,12}, B. Bassett^{13,14}, A. Becker¹⁵, D. Cinabro¹⁶, F. DeJongh¹⁷,
B. Dilday^{18,19}, M. Doi²⁰, J. A. Frieman^{11,17,18}, C. J. Hogan¹⁵, J. Holtzman²¹, S. Jha²²,
R. Kessler^{19,23}, K. Konishi²⁴, H. Lampeitl²⁵, J. Marriner¹⁷, J. L. Marshall⁵, G. Miknaitis¹⁷,
R. C. Nichol²⁶, A. G. Riess^{25,27}, M. W. Richmond²⁸, R. Romani²², M. Sako²⁹,
D. P. Schneider³⁰, M. Smith²⁶, N. Takanashi²⁰, K. Tokita²⁰, K. van der Heyden¹³,
N. Yasuda²⁴, C. Zheng²², J. C. Wheeler,³¹ J. Barentine^{31,32}, J. Dembicky³², J. Eastman⁵,
S. Frank⁵, W. Ketzeback³², R. J. McMillan³², N. Morrell⁷, G. Folatelli⁷, C. Contreras⁷,
C. R. Burns³³, W. L. Freedman³³, S. González⁷, M. Hamuy³⁴, W. Krzeminski⁷,
B. F. Madore³³, D. Murphy¹³, S. E. Persson³³, M. Roth⁷, N. B. Suntzeff³⁵

¹Based in part on observations obtained with the Apache Point Observatory 3.5-meter telescope, which is owned and operated by the Astrophysical Research Consortium.

²Based in part on observations taken at the Cerro Tololo Inter-American Observatory, National Optical Astronomy Observatory, which is operated by the Association of Universities for Research in Astronomy, Inc. (AURA) under cooperative agreement with the National Science Foundation.

³This paper includes data gathered with the 6.5 meter Magellan Telescopes located at Las Campanas Observatory, Chile.

⁴Partly based on observations collected at the European Southern Observatory, Chile, in the course of programme 076.A-0156.

⁵ Department of Astronomy, Ohio State University, 140 West 18th Avenue, Columbus, OH 43210-1173.

⁶ University of Notre Dame, 225 Nieuwland Science, Notre Dame, IN 46556-5670.

⁷ Las Campanas Observatory, Carnegie Observatories, La Serena, Chile

⁸ Holmer L. Dodge Department of Physics and Astronomy, University of Oklahoma, 440 West Brooks, Room 100, Norman, OK 73019-2061

⁹ Astronomy Department, University of California at Berkeley, 601 Campbell Hall, Berkeley, CA 94720

¹⁰ Chandra Fellow

¹¹ Department of Astronomy and Astrophysics, The University of Chicago, 5640 South Ellis Avenue, Chicago, IL 60637.

¹² Computational Research Division, Lawrence Berkeley National Laboratory, MS 50F-1650, 1 Cyclotron Rd, Berkeley, CA 94720 USA

¹³ Department of Mathematics and Applied Mathematics, University of Cape Town, Rondebosch 7701, South Africa.

¹⁴ South African Astronomical Observatory, P.O. Box 9, Observatory 7935, South Africa.

¹⁵ Department of Astronomy, University of Washington, Box 351580, Seattle, WA 98195.

¹⁶ Department of Physics, Wayne State University, Detroit, MI 48202.

¹⁷ Center for Particle Astrophysics, Fermi National Accelerator Laboratory, P.O. Box 500, Batavia, IL 60510.

¹⁸ Kavli Institute for Cosmological Physics, The University of Chicago, 5640 South Ellis Avenue Chicago, IL 60637.

¹⁹ Department of Physics, University of Chicago, Chicago, IL 60637.

²⁰ Institute of Astronomy, Graduate School of Science, University of Tokyo 2-21-1, Osawa, Mitaka, Tokyo 181-0015, Japan.

²¹ Department of Astronomy, MSC 4500, New Mexico State University, P.O. Box 30001, Las Cruces, NM 88003.

prieto@astronomy.ohio-state.edu

ABSTRACT

We present extensive *ugrizYHJK_s* photometry and optical spectroscopy of SN 2005gj obtained by the SDSS-II and CSP Supernova Projects, which give excellent coverage during the first 150 days after the time of explosion. These data show that SN 2005gj is the second clear case, after SN 2002ic, of a thermonuclear explosion in a dense circumstellar environment. Both the presence of singly and doubly ionized iron-peak elements (Fe III and weak S II, Si II) near maximum light as well as the spectral evolution show that SN 2002ic-like events are Type Ia explosions. Independent evidence comes from the exponential decay in luminosity of SN 2005gj, pointing to an exponential density distribution of the ejecta. The interaction of the supernova ejecta with the dense circumstellar

²² Kavli Institute for Particle Astrophysics & Cosmology, Stanford University, Stanford, CA 94305-4060.

²³ Enrico Fermi Institute, University of Chicago, 5640 South Ellis Avenue, Chicago, IL 60637.

²⁴ Institute for Cosmic Ray Research, University of Tokyo, 5-1-5, Kashiwanoha, Kashiwa, Chiba, 277-8582, Japan.

²⁵ Space Telescope Science Institute, 3700 San Martin Drive, Baltimore, MD 21218.

²⁶ Institute of Cosmology and Gravitation, Mercantile House, Hampshire Terrace, University of Portsmouth, Portsmouth PO1 2EG, UK.

²⁷ Department of Physics and Astronomy, Johns Hopkins University, 3400 North Charles Street, Baltimore, MD 21218.

²⁸ Physics Department, Rochester Institute of Technology, 85 Lomb Memorial Drive, Rochester, NY 14623-5603.

²⁹ Department of Physics and Astronomy, University of Pennsylvania, 203 South 33rd Street, Philadelphia, PA 19104.

³⁰ Department of Astronomy and Astrophysics, The Pennsylvania State University, 525 Davey Laboratory, University Park, PA 16802.

³¹ Department of Astronomy, McDonald Observatory, University of Texas, Austin, TX 78712

³² Apache Point Observatory, P.O. Box 59, Sunspot, NM 88349.

³³ Carnegie Institution of Washington, 813 Santa Barbara St., Pasadena, CA 91101

³⁴ Universidad de Chile, Departamento de Astronomía, Santiago, Chile

³⁵ Texas A&M University Physics Department, College Station, TX

medium is stronger than in SN 2002ic: (1) the supernova lines are weaker; (2) the Balmer emission lines are more luminous; and (3) the bolometric luminosity is higher close to maximum light. The velocity evolution of the H α components suggest that the CSM around SN 2005gj is clumpy and it has a flatter density distribution compared with the steady wind solution, in agreement with SN 2002ic. An early X-ray observation with *Chandra* gives an upper-limit on the mass loss rate from the companion of $\dot{M} \lesssim 2 \times 10^{-4} \text{ M}_{\odot} \text{ yr}^{-1}$.

Subject headings: supernovae: general — supernovae: individual (SN 2005gj)

1. Introduction

Thermonuclear supernova explosions (Type Ia supernovae, SN Ia hereafter) are believed to be the detonation or deflagration of a white dwarf accreting matter from a companion star (Arnett 1982). The mass of the white dwarf slowly increases until it approaches the Chandrasekhar limit where the star becomes thermally unstable. At this point fusion of Carbon and Oxygen begins near the center and quickly moves through most of the star before degeneracy is lifted. The result is a spectacular and powerful explosion that is visible across much of the Universe. Since SN Ia arise from a narrow range of white dwarf masses, their peak luminosities are very consistent and they make excellent distance indicators (e.g., Phillips 1993). SN Ia are powerful probes of cosmology and have been instrumental in narrowing the uncertainty in the Hubble parameter, discovery of the accelerating universe, and constraining dark energy models (Hamuy et al. 1995, 1996b; Riess et al. 2005, 1998; Perlmutter et al. 1999; Riess et al. 2004; Astier et al. 2006; Riess et al. 2006; Wood-Vasey et al. 2007).

But the use of SN Ia as reliable distance indicators will always be questioned until the progenitor and explosion physics are well-understood. What types of binaries create SN Ia? How is matter transferred to the white dwarf without causing thermonuclear runaways on the surface? Are there several types of progenitors?. These big questions remain to be answered and detailed observations of hundreds of events have yielded few clues.

In 2002, Hamuy et al. (2003) identified a new kind of supernova. The early spectrum of SN 2002ic was a cross between a Type Ia event and a Type IIn (Deng et al. 2004, have called this type of supernova a “IIa”), showing P-Cygni features similar to SN Ia and resolved Balmer lines in emission. Type IIn supernovae are core-collapse explosions going off in dense circumstellar environments (Schlegel 1990; Chevalier & Fransson 1994). They are relatively common since the massive stars that create core-collapse supernovae often have thick winds. If the interpretations of the pre-explosion observations of SN 2005gl are correct, SN IIn could

be associated in some cases with luminous blue variables (Gal-Yam et al. 2006).

In the case of SN 2002ic, the presence of Balmer lines with profiles characteristic of SN IIn, and the high luminosities and slow decline after maximum lead to the conclusion that most of the energy came from the interaction of the ejecta with a dense circumstellar medium (CSM). Other Type IIn events (SN 1997cy, Germany et al. 2000; SN 1999E, Rigon et al. 2003) have been re-classified as SN 2002ic-like that were caught late in their evolution (Hamuy et al. 2003; Wood-Vasey et al. 2004).

SN 2002ic provided the first direct evidence that thermonuclear explosions can also occur in a dense medium, but in this case the circumstellar medium is probably generated by an Asymptotic Giant companion (Hamuy et al. 2003; Wang et al. 2004; Han & Podsiadlowski 2006). However, there is still debate in the literature about the origin of SN 2002ic. Livio & Riess (2003) proposed the merger of two white dwarfs as a possible progenitor, with the explosion occurring in the common envelope phase. Chugai et al. (2004) concluded that the properties of the circumstellar interaction in 2002ic-like events can be broadly explained by the SN 1.5 scenario (Iben & Renzini 1983): the thermonuclear explosion of the degenerate core of a massive AGB star. Recently, Benetti et al. (2006) questioned the earlier interpretation of the observations and proposed that SN 2002ic can be equally well explained by the core collapse of a stripped-envelope massive star in a dense medium.

SN 2005gj was discovered on 2005 September 28.6 (UT) by the SDSS-II Supernova Collaboration (Frieman et al. 2007) in *gri* images obtained with the SDSS-2.5m telescope at Apache Point Observatory (APO). The new supernova (Barentine et al. 2005) was $\sim 1''$ from the center of its host galaxy at the position $\alpha = 03^{\text{h}}01^{\text{m}}12^{\text{s}}.0$, $\delta = +00^{\circ}33'13''.9$ (J2000.0). It had SDSS magnitudes $(g, r, i) = (18.6, 18.6, 18.7)$ mag, obtained from PSF photometry after kernel-matching and subtraction of a template image in each band. The SN was independently discovered by the Nearby Supernova Factory on 2005 September 29 (Aldering et al. 2006).

SN 2005gj was classified as a Type Ia candidate from the first three epochs of the *gri* light curve using a light curve fitting program, and was sent to the queue of the MDM-2.4m telescope for spectroscopic confirmation. The optical spectrum obtained on 2005 October 1 (UT) showed a blue continuum with resolved Hydrogen Balmer lines in emission, very similar to the spectrum of a young Type IIn supernova, but also with an unusual continuum showing broad and weak absorption features. Further spectroscopic follow-up showed a dramatic evolution. The continuum became substantially redder and developed broad, P-Cygni features probably associated with blended lines of Fe-peak mass elements, similar to a Type Ia SN a few weeks after maximum. The spectrum obtained on 2005 Nov. 12 (UT) was remarkably similar to that of the unusual Type Ia supernova SN 2002ic obtained on 2002

Dec. 27 (UT) (Prieto et al. 2005).

Aldering et al. (2006) presented optical photometry and spectroscopy of this SN. Through detailed analysis they confirmed its photometric and spectroscopic resemblance to SN 2002ic, confirming it was a new case of a Type Ia explosion interacting with a dense circumstellar environment. From a spectrum obtained with the slit oriented to overlap with its host galaxy, they calculated a redshift for the host of $z = 0.0616 \pm 0.0002$. SN 2005gj was not detected in the radio with the Very Large Array (Soderberg & Frail 2005) or in the X-ray with *Swift* (Immler et al. 2005).

Here we present extensive follow-up photometry and spectroscopy of the Type Ia/Type IIn SN 2005gj during the first ~ 150 days after discovery. These are the most detailed observations ever obtained of a SN 2002ic-like event, and provide insight into the early evolution, progenitor, and variety of these events. We also present a sensitive, early X-ray observation with *Chandra* that gives an upper limit on the X-ray luminosity of this peculiar object. We describe the optical and NIR photometry of SN 2005gj in § 2 and the optical spectroscopy in § 3. We describe the X-ray observation with *Chandra* in § 4. An analysis of the photometric and spectroscopic data are presented in § 5. Finally, we discuss the significance of the results in § 6. We will present later photometric follow-up and Spitzer/IRAC observations in Paper II. We adopt a cosmology with $H_0 = 72 \pm 8 \text{ km s}^{-1} \text{ Mpc}^{-1}$, $\Omega_M = 0.3$, and $\Omega_\Lambda = 0.7$ throughout the paper (see Spergel et al. 2006), which yields a distance modulus of $\mu = 37.15 \text{ mag}$ to the host of SN 2005gj.

2. Photometry

2.1. SDSS and MDM

The Sloan Digital Sky Survey (SDSS; York et al. 2000) uses a wide-field, 2.5-meter telescope (Gunn et al. 2006) and mosaic CCD camera (Gunn et al. 1998) at APO to survey the sky. The SDSS-II Supernova Survey, part of a 3-year extension of the original SDSS, uses the APO-2.5m telescope to detect and measure light-curves for a large number of supernovae through repeat scans of the SDSS Southern equatorial stripe (about 2.5 deg wide by ~ 120 deg long) over the course of three 3-month campaigns (Sept-Nov. 2005-2007). SN 2005gj was discovered in the second month of the first campaign (October 2005). Twenty epochs of *ugriz* photometry were obtained between 2005 Sep 26-Nov 30 (U.T.). Details of the photometric system, magnitude system, astrometry and calibration are given in Fukugita et al. (1996), Lupton et al. (1999), Hogg et al. (2001), Smith et al. (2002), Pier et al. (2003), Ivezić et al. (2004), and Tucker et al. (2006). Additional *griz* imaging of

SN 2005gj was obtained with the MDM Observatory 2.4m telescope using a facility CCD imager (RETROCAM; see Morgan et al. 2005, for a complete description of the imager).

Photometry of SN 2005gj on the SDSS images was carried out using the scene modeling code developed for SDSS-II as described in Holtzman et al. (2007). A sequence of stars around the supernova were taken from the list of Ivezić et al. (2007), who derived standard SDSS magnitudes from multiple observations taken during the main SDSS survey under photometric conditions. Using these stars, frame scalings and astrometric solutions were derived for each of the supernova frames, as well as for the twenty five pre-supernova frames taken as part of either the main SDSS survey or the SN survey. Finally, the entire stack of frames was simultaneously fit for a single supernova position, a fixed galaxy background in each filter (characterized by a grid of galaxy intensities), and the supernova brightness in each frame.

The supernova photometry in the MDM frames was also determined using the scene modeling code. Since the MDM observations had different response functions from the standard SDSS bandpasses, the photometric frame solutions included color terms from the SDSS standard magnitudes. To prevent uncertainties in the frame parameters and color terms from possibly corrupting the galaxy model (here affecting the SDSS photometry), the MDM data were not included in the galaxy determination, but the galaxy model as determined from the SDSS was used (with color terms) to subtract the galaxy in the MDM frames. The resulting SN photometry from the MDM frames is reported on the native MDM system, since the color terms derived from stars are likely not to apply to the spectrum of the supernova.

Figure 1 shows a $3.5' \times 3.5'$ field around SN 2005gj and 16 comparison stars used for calibration of the SN magnitudes by SDSS and the Carnegie Supernova Group (CSP; see § 2.2 below for details). In Table 1 we present the SDSS *ugriz* and CSP *u'g'r'i'* photometry of the comparison stars in common. The final SDSS and MDM *griz* photometry is given in Table 2.

2.2. CSP

Optical photometry from the CSP was obtained with the Swope-1m telescope at LCO, using a SiTe CCD and a set of *u'g'r'i'* filters. A subraster of 1200×1200 pixels was read from the center of the CCD, which, at a scale of $0.435'' \text{ pixel}^{-1}$, yielded a field of view of $8.7' \times 8.7'$. Typical image quality ranged between $1''$ and $2''$ (FWHM). A photometric sequence of comparison stars in the SN field was calibrated with the Swope telescope from

observations of SDSS standard stars from Smith et al. (2002) during four photometric nights. SN magnitudes in the $u'g'r'i'$ system were obtained differentially relative to the comparison stars using PSF photometry. In order to minimize the contamination from the host galaxy light in the SN magnitudes, PSF-matched $ugri$ template images from SDSS were subtracted from the SN images. On every galaxy-subtracted image, a PSF was fitted to the SN and comparison stars within a radius of $3''$. See Hamuy et al. (2006) for further details about the measurement procedures.

The NIR photometry of SN 2005gj was obtained by the CSP using three different instruments/telescopes. A total of 15 epochs in Y , J and H filters were obtained using RetroCam, mounted on the Swope-1m telescope at LCO. A few additional epochs in $YJHK_s$ were obtained with the Wide Infrared Camera (WIRC; Persson et al. 2002) mounted on the duPont-2.5m telescope, and the PANIC camera (Martini et al. 2004) mounted on the Magellan-6.5m Baade telescope, both at LCO. We refer to Hamuy et al. (2006) and Phillips et al. (2007) for details of the imagers and procedures to extract the SN photometry. The host galaxy was not subtracted from the NIR frames; therefore the SN photometry contains an unknown galaxy contamination component.

The final CSP $u'g'r'i'$ photometry of SN 2005gj is given in Table 3 and $YJHK_s$ photometry in Table 4. A minimum uncertainty of 0.015 mag in the optical bandpasses and 0.02 mag in the NIR is assumed for a single measurement based on the typical scatter in the transformation from instrumental to standard magnitudes of bright stars (Hamuy et al. 2006).

3. Spectroscopy

The spectroscopic observations of SN 2005gj are summarized in Table 6. They were obtained using five different telescopes/instruments at four observatories.

A total of twelve spectra were obtained between early-October 2005 and late-January 2006 with the Boller & Chivens CCD Spectrograph (CCDS) mounted at the MDM-2.4m telescope. This instrument uses a Loral 1200×800 pixel CCD with $15 \mu\text{m pixel}^{-1}$ and a 150 l/mm grating (blazed at 4700 \AA). We used a $2''$ slit which gives a dispersion of $3.1 \text{ \AA pixel}^{-1}$ in the wavelength range $\sim 3800\text{--}7300 \text{ \AA}$.

Eight spectra were obtained at LCO with the Wide Field Reimaging Camera (WFCCD) and the Modular Spectrograph (ModSpec) at the duPont-2.5m telescope, and LDSS-3 at the Clay-6.5m telescope. In the case of WFCCD a 400 l/mm grism and a $1.6''$ slit were used, reaching a dispersion of 3 \AA pixel^{-1} in the wavelength range $\sim 3800\text{--}9200 \text{ \AA}$. For ModSpec we

used a 300 l/mm grating and a 1'' slit that gave a dispersion of $2.45 \text{ \AA pixel}^{-1}$ in the range $\sim 3800\text{--}7300 \text{ \AA}$. Further details of WFCCD and ModSpec can be found in Hamuy et al. (2006). For LDSS-3, which employs a STA0500A 4064×4064 pixel CCD, we used the VPH blue and red grisms, the latter with an OG590 filter to block second order contamination, with a 0.75'' slit reaching a dispersion of $0.70 \text{ \AA pixel}^{-1}$ and $1.12 \text{ \AA pixel}^{-1}$ in the blue and red sides of the spectrum, respectively.

Additionally we obtained two early spectra with the Double Imaging Spectrograph (DIS) mounted on the ARC-3.5m telescope at APO, and one spectrum with the Intermediate dispersion Spectrograph and Imaging System (ISIS) at the WHT-4.2m telescope at the Roque de Los Muchachos Observatory in La Palma, Spain. The DIS spectrograph has blue and red detectors, each uses a Marconi 2048×1024 pixel CCD with $13.5 \mu\text{m pixel}^{-1}$. We used a 300 l/mm grating and a 1.5'' slit which gives a dispersion of $2.4 \text{ \AA pixel}^{-1}$. The ISIS spectrograph has a blue and red arm, the blue arm using a EEV12 CCD and the red using a MARCONI2 detector. We used a 300 l/mm grating in both the blue and red arm and a 1'' slit, which gives a dispersion of $0.86 \text{ \AA pixel}^{-1}$ in the blue and $1.47 \text{ \AA pixel}^{-1}$ in the red.

Most of the spectra were obtained close to the parallactic angle to minimize relative changes in the calibration of the blue and red parts of the spectrum due to differential refraction through the atmosphere. The spectroscopic reductions were performed using standard IRAF tasks and included: bias and overscan subtraction, flat-fielding, combination of 2-4 individual 2D spectra to reach the best signal-to-noise ratio in the final image, tracing and extraction of a 1D spectrum from the combined 2D image, subtracting the background sky around the selected aperture, wavelength calibration using an arc-lamp, and flux calibration. In order to flux calibrate the spectra we observed 1-2 spectrophotometric standard stars per night. The spectra from LCO, WHT and MDM were corrected by atmospheric telluric lines using the spectrum of a hot spectrophotometric standard star and the spectra from APO were corrected using a model atmosphere. This correction is not optimal for some of the spectra and there are evident residuals left in the corrected spectra.

Figure 2 and 3 show a montage of the optical spectra of SN 2005gj obtained from October 2005 to March 2006. We have split them in two figures to avoid crowding. The position of the most conspicuous spectral features have been indicated in this figure.

4. X-ray Observation

SN 2005gj was observed under Director's Discretionary Time for 49.5 ks on 2005 Dec 11/12 (ObsID 7241) with the *Chandra X-ray Observatory's* Advanced CCD Imaging Spec-

trometer (ACIS). The data were taken in timed-exposure mode with an integration time of 3.2 s per frame, and the telescope aimpoint was on the back-side illuminated S3 chip. The data were telemetered to the ground in “very faint” mode.

Data reduction was performed using the CIAO 3.3 software provided by the *Chandra* X-ray Center¹. The data were reprocessed using the CALDB 3.2.2 set of calibration files (gain maps, quantum efficiency, quantum efficiency uniformity, effective area) including a new bad pixel list made with the `acis_run_hotpix` tool. The reprocessing was done without including the pixel randomization that is added during standard processing. This omission slightly improves the point spread function. The data were filtered using the standard *ASCA* grades (0, 2, 3, 4, and 6) and excluding both bad pixels and software-flagged cosmic ray events. Intervals of strong background flaring were searched for, but none were found.

Absolute *Chandra* astrometry is typically good to $\sim 0''.5$, and we sought to improve it by registering the *Chandra* image with an SDSS image. *Chandra* point sources were found using the `wavdetect` tool, and their positions were refined using ACIS Extract version 3.101. Fourteen X-ray sources had SDSS counterparts, which we used to shift the *Chandra* frame by a small amount ($0''.15$ in RA and $0''.07$ in DEC). After the shift, the residual differences between the *Chandra* and SDSS sources had rms values of $0''.19$ in RA and $0''.12$ in DEC.

We extracted counts in the 0.5–8 keV bandpass from the position of the supernova using a standard extraction region ($\sim 1''$ radius), and we constructed response files with the CIAO tools and ACIS Extract. The background region is a source-free annulus centered on the position of the supernova with inner and outer radii of $6''$ and $32''$. Based on the 300 photons detected in this region, we expect 0.3 background counts in our source extraction region.

We detect only two counts from the location of the supernova, but neither may be associated with the supernova itself. The counts had energies of 4.0 keV and 6.5 keV, but one would expect some emission in the 0.5–2.5 keV range since this is where *Chandra* has the most collecting area. For example, the average effective area in each of the 0.5–2.5 keV, 4.0–6.0 keV, and 6.0–8.0 keV bands is 470 cm², 270 cm², and 90 cm², respectively.

We calculate our upper limits using the Bayesian method of Kraft et al. (1991). For the 0.5–4 keV band, the 68% (95.5%) upper limit to the source counts is 1.14 (3.05). For the 0.5–8 keV band, the 68% (95.5%) upper limit is 3.52 (6.14).

Since no Type Ia supernova has been conclusively detected in X-ray, we have no *a priori* expectation of the spectral shape. We therefore adopt a simple absorbed power law with a photon index of 2 and an absorbing column of $n_H = 7.08 \times 10^{20}$ cm⁻². For this choice of

¹<http://asc.harvard.edu>

spectrum, the count rate to flux conversion is 5.2×10^{-12} erg/count in the 0.5–4 keV band and 6.9×10^{-12} erg/count in the 0.5–8 keV band.

We therefore arrive at 68% (95.5%) upper limits on the X-ray luminosity of 1.1 (2.9) $\times 10^{39}$ erg s $^{-1}$ in the 0.5–4 keV band and 4.3 (7.6) $\times 10^{39}$ erg s $^{-1}$ in the 0.5–8 keV band. Based on the above statements concerning the *Chandra* effective area, we feel the 0.5–4 keV limit is a more appropriate limit.

5. Results

5.1. Optical light curves and colors

Figure 4 shows the early SDSS and MDM *ugriz* light curves combined with the late time coverage given by CSP *u'g'r'i'YJHK_s* photometry. They give excellent multi-wavelength optical and NIR coverage and sampling of the first ~ 150 days after discovery (~ 140 rest-frame days after the time of explosion).

In Table 5 we give important parameters derived from the light curves. We have a good estimate of the time of explosion of the SN at JD 2,453,637.93 \pm 2.02 (September 24.4 UT, 2005) calculated as the average time between the epoch when the supernova is detected at $> 5\sigma$ in all filters at JD 2,453,639.94, and the last pre-discovery observation of the field at JD 2,453,635.91. The times and observed magnitudes at maximum in different filters are presented in Table 5. They are calculated from a high order polynomial fit to each light curve. To estimate the errors we assume a gaussian distribution for the magnitude uncertainty at each epoch and filter (assuming they are not correlated from epoch to epoch), then we draw randomly ~ 1000 simulated light curves and fit each one with the same high order polynomial. The 1σ uncertainties are taken as the rms deviation of the mean values calculated from each simulated light curve.

The risetimes, defined as the time between explosion and maximum light, become longer at redder wavelengths. They are 13.5, 19.7, 33.7, and 46.9 days in *ugri* filters, respectively, which correspond to 12.7, 18.5, 31.7, and 44.2 days in the rest-frame of the supernova.

We also give in Table 5 the rest-frame magnitudes at maximum in different filters. They have been corrected by Galactic extinction in the line of sight, using $E(B - V)_{Gal} = 0.121$ (SFD: Schlegel et al. 1998) and the Cardelli et al. (1989) (CCM) reddening law assuming $R_V = 3.1$, and *K*-corrections (see below), which are not negligible in this object since it is at redshift $z \sim 0.062$. We assume that the host galaxy extinction is negligible (Aldering et al. 2006).

K -corrections have been calculated from the multi-epoch spectra presented in § 3. In order to estimate accurate K -corrections we need good spectrophotometric calibration in all the wavelength range. Figure 5 shows the differences between the observed $g-r$ photometric colors obtained from the light curves and the synthetic colors calculated directly from the spectra, as a function of the observed photometric colors. We use an 8th order polynomial fit of the light curves to obtain the observed $g-r$ color at the epoch of a given spectrum to better than ~ 0.03 mag. We can see that most of the spectra have good spectrophotometric calibration in the wavelength range of g, r filters (3800–7000 Å), with a residual color of ~ 0.05 mag rms (difference between observed and synthetic colors), but there are some obvious outliers. To correct the spectra and produce a better spectrophotometric calibration consistent with the observed spectral energy distribution (SED) obtained from broadband photometry we *warp* the spectra multiplying by a smooth function to match the observed colors, a technique commonly used for calculating K -corrections in Type Ia SN (Nugent et al. 2002).

First, we extrapolate the continuum in the blue and red sides of each spectrum presented in § 3 with a low order polynomial to have complete coverage of the SDSS *ugriz* filters (2000–11000 Å). Using this extended version of the spectra we apply the CCM reddening law iteratively until the synthetic $g-r$ color matches the observed color in each spectrum. This procedure does not ensure that the calibration is good in the complete wavelength range; therefore we multiply by a smooth spline with knots at the effective wavelength of the SDSS filters until the synthetic $u-g$, $g-r$, $r-i$ and $i-z$ colors match the observed colors obtained, again by using polynomial interpolation of the light curves.

The K -corrections for the same filter (Hamuy et al. 1993) calculated from the modified, spectrophotometrically calibrated spectra using SDSS passbands are listed in Table 7. The K -corrections are probably accurate to ± 0.05 mag for g and r filters, and to ± 0.1 mag for u , i and z where we had to extrapolate the spectra. However, our estimate is not precise and we can not exclude the possibility of even larger errors. After fitting with a low order polynomial we use the results to transform the observed SDSS magnitudes in Table 2 to the rest-frame.

We corrected the CSP $u'g'r'i'$ magnitudes to rest-frame SDSS *ugri* magnitudes using cross-filter K -corrections according to the prescription of Nugent et al. (2002). These take into account the difference between the CSP and SDSS passbands convolved by the SED of SN 2005gj and allow us to put all the rest-frame magnitudes in the same system. We find that the differences between the same- and cross-filter K -corrections are small ($\lesssim 0.03$ mag) at all epochs.

Figure 6 shows the evolution of the rest-frame colors of SN 2005gj as a function of time

after explosion. We have corrected the magnitudes by K -corrections and Galactic extinction in the line of sight. As a comparison we also plot the color evolution of the overluminous Type Ia SN 1991T, a typical Type IIn SN 1999el (Di Carlo et al. 2002) (both obtained from spectral templates of P. Nugent ²), and two previous cases that are thought to be Type Ia explosions in a very dense environment: SN 2002ic and SN 1997cy. For SN 2002ic we use the published BVI photometry (Hamuy et al. 2003) corrected by Galactic extinction ($E(B - V) = 0.06$; SFD). We calculate cross-filter K -corrections using the calibrated spectra of SN 2005gj to transform observed magnitudes of the SN at $z = 0.0667$ (Kotak et al. 2004) to rest-frame SDSS magnitudes: $B \rightarrow u$, $V \rightarrow g$, $I \rightarrow i$. The time of explosion of SN 2002ic is assumed to be at \approx JD 2,452,581.5 (2002, Nov. 3 UT; Deng et al. 2004). We obtain rest-frame colors in the SDSS system for SN 1997cy (Germany et al. 2000; Turatto et al. 2000) by transforming the K -corrected VRI magnitudes in Germany et al. (2000) to gri magnitudes using S -corrections calculated directly from spectra of SN 1997cy available online in the SUSPECT database ³. We supplement this with synthetic colors from the spectra. We also correct by Galactic extinction in the line of sight ($E(B - V) = 0.02$; SFD) and assume the time of explosion of SN 1997cy to be JD 2,450,582.5 (1997, May. 14 UT; Germany et al. 2000), which is very uncertain, since it is taken as the time of detection of the gamma-ray burst GRB 970514, which may not have been associated with the SN. Magnitudes for SN 2002ic and SN 1997cy are not corrected by extinction in their host galaxies, which is unknown.

Initially the evolution in rest-frame $u - g$ and $g - r$ colors of SN 2005gj, up to ~ 30 -40 days after explosion (~ 10 -20 days after maximum for a SN Ia), is roughly consistent with the colors of SN 1991T but ~ 0.2 mag redder in $g - r$, and evolves to redder colors at later times. SN 1991T reaches its maximum colors of $(u - g) = 1.5$ mag and $(g - r) = 1.0$ mag at ~ 50 days (30 days after maximum), and after that it enters the nebular phase and becomes bluer. At late times the $u - g$ color of SN 2005gj has a slow linear increase and becomes systematically redder than SN 1991T at > 70 days, while the $g - r$ color stays approximately flat at $(g - r) = 0.5$ mag (and bluer than SN 1991T) between 60 – 110 days. The evolution in $u - g$ color of SN 2002ic is very similar and consistent with SN 2005gj. SN 1997cy has a similar color evolution but it is ~ 0.2 mag bluer in $g - r$ color between 60 – 100 days. However, Germany et al. (2000) give K -correction errors of ~ 0.15 mag and we have further applied S -corrections, therefore this does not imply a significant difference between SN 1997cy and the other two Type Ia/IIn supernovae.

²http://supernova.lbl.gov/~nugent/nugent_templates.html

³<http://suspect.nhn.ou.edu/~suspect/>

The rest-frame $r - i$ and $i - z$ color evolution of SN 2005gj is very different from SN 1991T and closely follows the evolution of a SN IIn. The $r - i$ colors of SN 1997cy are also consistent with SN 2005gj. From these comparisons it is clear that the colors, a proxy for the temperature of the photosphere, of SN 2005gj and two earlier cases of SN Ia strongly interacting with their circumstellar medium are dominated by the radiation coming from the ejecta-CSM interaction.

In Figure 7 we present the *ugri* light curves of SN 2005gj in absolute magnitudes. We also show the light curves of SN 1991T, SN 2002ic and SN 1997cy obtained from the literature and corrected to SDSS rest-frame magnitudes as explained above.

SN 2005gj has peak *ugriz* absolute magnitudes in the range -20.0 to -20.3 mag, this is ~ 0.7 – 1.4 mag brighter than the overluminous Type Ia SN 1991T. The *u* light curve is consistent with a linear decline after peak luminosity at a constant rate of 0.027 ± 0.001 mag day $^{-1}$. The *g* light curve has a ~ 20 day plateau with roughly constant luminosity after maximum (20–40 days after explosion), then the light curve declines linearly between 40–100 days at 0.018 ± 0.001 mag day $^{-1}$ and continues its linear decay at later times, but with a shallower slope of 0.007 ± 0.002 mag day $^{-1}$. The *r* and *i* light curves have a similar plateau shape between 20–60 days and a constant linear decay at later times of 0.013 ± 0.001 mag day $^{-1}$. The change in slope observed in the *g*-band at late times is less clear in *ri*, but still present. The secondary maximum present in *ri* light curves of SN 1991T and other SN Ia is completely absent in SN 2005gj.

The light curves of SN 2002ic are fainter than SN 2005gj at all times by 0.3 – 0.6 mag depending on the filter (0.3 – 0.8 mag brighter than SN 1991T at peak). The initial decline rates from maximum of the *u* and *g* light curves of SN 2002ic are intermediate between those of SN 1991T and SN 2005gj until around 40 days after explosion; after day 50 when the ejecta-CSM interaction had become dominant in SN 2002ic (Hamuy et al. 2003), they closely resemble the decline rates of SN 2005gj in the same bands. The *i* band light curve of SN 2002ic showed definite evidence for a weak secondary maximum, which is again intermediate in morphology between the strong secondary maximum observed in SN 1991T, and the absence of such a feature in SN 2005gj. The *gr* light curves of SN 1997cy are consistent with linear decay of ~ 0.008 mag day $^{-1}$, being ~ 0.4 mag brighter than SN 2005gj at 150 days. Unfortunately, the light curves of SN 1997cy start at ~ 60 days after explosion and there is no information near peak to compare with the luminosities of SN 2005gj and SN 2002ic. However, if we extrapolate the *gr* light curves to the time of peak luminosity we find that the absolute magnitudes at maximum of SN 1997cy would be within ~ 0.2 mag of SN 2005gj. This has to be taken with caution because of the extrapolation and uncertain time of explosion of SN 1997cy.

5.2. NIR light curves

We used the CSP JHK_s photometry obtained between 59-166 days after the explosion (rest-frame) to construct the absolute magnitude light curves of SN 2005gj. The observed magnitudes were corrected by Galactic reddening in the line of sight ($A_J = 0.108$, $A_H = 0.070$, and $A_{K_s} = 0.044$ mag) and K -corrections. We calculated K -corrections for the same filter using the spectral templates of P. Nugent for the Type IIn SN 1999el (which are derived from black-body curve fits to the photometry), because as we showed in § 5.1 the synthetic colors obtained from the spectral templates approximate reasonably well the evolution of the redder optical colors of SN 2005gj (i.e., $r - i$ and $i - z$). The values of the K -corrections are consistent with being constant in this time range: $K_J \approx -0.12$ mag, $K_H \approx -0.14$ mag, $K_{K_s} \approx 0.16$ mag.

The JHK_s absolute magnitude light curves of SN 2005gj are presented in Figure 8. For comparison we show the NIR light curves of a normal Type Ia obtained from synthetic photometry of spectral templates and the Type IIn SN 1999el (Di Carlo et al. 2002). The Type Ia light curves have been shifted in magnitudes to match the mean absolute magnitude at maximum of SN Ia (Krisciunas et al. 2004). SN 2005gj is 1.7 – 3 mag brighter than a normal SN Ia and SN IIn at 60 days after the explosion and declines in a slower fashion at later times. A linear decay is a good fit in all NIR bandpasses at this late times (> 60 days after explosion), with decline rates of ~ 0.014 mag day $^{-1}$ in J , ~ 0.013 mag day $^{-1}$ in H , and ~ 0.011 mag day $^{-1}$ in K_s . These values are similar to the decline rates in the optical ri bands.

Since there are no template images of the host galaxy obtained in the NIR bands, the light curves are preliminary and the analysis has to be taken with caution.

5.3. Bolometric light curve

The SDSS and CSP magnitudes were used to produce a quasi-bolometric light curve of SN 2005gj covering the optical wavelength range from 3000 – 10,000 Å ($u \rightarrow z$). We corrected the magnitudes by Galactic extinction in the line of sight and K -corrections to obtain magnitudes in the rest-frame $ugriz$ filters (see § 5.1 for details). We applied small corrections to transform the magnitudes based in the SDSS photometric system into the AB system obtained from the SDSS website ⁴. The AB magnitudes derived in this way are transformed directly to bandpass averaged fluxes using the definition of the AB system

⁴<http://www.sdss.org/dr5/algorithms/fluxcal.html>.

(Oke & Gunn 1983) and they are assigned to the frequencies that correspond to the effective wavelengths of the SDSS *ugriz* filters, calculated from the filters using the definition in Fukugita et al. (1996): 3567, 4735, 6195, 7510, and 8977 Å. We use the trapezoidal rule to obtain the integrated flux from *u* to *z*, this is between $\lambda_1 = 3340$ Å and $\lambda_2 = 9596$ Å, where the limits of the wavelength coverage are obtained from $\lambda_1 = \lambda_{eff,u} - \Delta\lambda_u/2$ and $\lambda_2 = \lambda_{eff,z} + \Delta\lambda_z/2$. We extrapolate linearly the *u* and *z* light curves at late times to fill in the lack of coverage of the SDSS in *z*, and CSP in *u* and *z* bands, including the MDM *z*-band data at these epochs. The integrated fluxes are converted to luminosity assuming a luminosity distance to SN 2005gj of 268.5 Mpc and a spherically symmetric distribution of the output energy. We present the integrated, quasi-bolometric luminosities from *u* to *i* ($L_{(u \rightarrow i)}$) and from *u* to *z* ($L_{(u \rightarrow z)}$) as a function of time in Table 8.

In order to estimate bolometric UVOIR luminosities we calculate time dependent *bolometric corrections* to include the energy output of the SN at wavelengths bluer than *u*-band ($\lambda < 3340$ Å) and redder than *z*-band ($\lambda > 9596$ Å). We find that black-body distributions with different temperatures are a reasonable approximation of the spectral energy distribution of SN 2005gj. We use χ^2 -minimization to fit the optical SED with a two parameter black-body function: temperature and a multiplicative scaling factor. The scaling factor is a combination of fundamental constants and the square of the angular radius of the spherical black-body: $(R_{bb}/d)^2$, where R_{bb} is the radius of the black-body and d is the distance to the SN. We calculate time-dependent bolometric corrections by integrating the black-body distributions in the ultraviolet and NIR/IR regions, and converting the integrated fluxes to luminosities as explained above. For the CSP data we also include NIR flux densities derived from the reddening and *K*-corrected *YJHK_s* magnitudes after fitting the light curves with low order polynomials.

At early phases before peak the bolometric corrections account for $\sim 53 - 65\%$ of the total integrated luminosity, of which $85 - 93\%$ is from the ultraviolet part of the spectrum and only $7 - 15\%$ from the NIR/IR. As the supernova evolves, the ejecta expands and shocks the circumstellar gas. The energy emitted in the ultraviolet/blue part of the spectrum declines quickly after maximum light and most of the energy is emitted in the optical region, coinciding with the appearance in the spectrum of emission/absorption features of the intermediate and iron-peak elements (see § 5.4). Between 25 – 150 days after explosion the bolometric corrections account for $\sim 32 - 45\%$ of the total output luminosity, with the NIR/IR correction dominating completely over the blue/ultraviolet at > 60 days.

The bolometric UVOIR luminosities, black-body temperatures and radii derived from the fits are presented in Table 8. The uncertainties in black-body temperatures and radii are calculated using the diagonal terms of the covariance matrix obtained from the χ^2 minimiza-

tion. We add a 10% error in the distance to the SN to the error in the black-body radii, which comes from the random and systematic uncertainties in the value of the Hubble constant (Freedman et al. 2001; Riess et al. 2005). The uncertainties in the bolometric luminosities were estimated by propagating errors through the trapezoidal integration of the SED, taking into account: uncertainties in the photometry, light curve interpolation and fitting, Galactic extinction, K -corrections, and distance to the SN. To approximately take into account the errors introduced by the bolometric corrections we multiplied these values by $\sqrt{\chi^2_\nu}$ when the reduced χ^2 is greater than 1.

In Figure 9 we show some examples of black-body fits to the optical SED at different epochs. At early times, shortly after explosion, the SED is very well fit by a hot ~ 13000 K black-body. The temperature starts to decrease steadily close to the time of explosion to a constant value of ~ 6500 K at 60 days after. A black-body is still a reasonable approximation of the SED at later times, but the fits become poorer when emission/absorption features start to dominate the spectrum, which is represented in the χ^2_ν of the fits (see Table 8).

Figure 10 shows the bolometric light curve of SN 2005gj in the top panel and the evolution in temperature and radius from the black-body fits in the lower panels. The early data of the bolometric light curve are well fit by an exponential rise in luminosity, $L(t) \propto e^{0.17t}$. The time of maximum bolometric luminosity occurs between 6.6–18.8 days after explosion. After maximum, the bolometric light curve is very well approximated by an exponential decay in luminosity, linear in the logarithmic scale shown in Figure 10, $L(t) \propto e^{-0.013t}$ ($0.014 \text{ mag day}^{-1}$). This is consistent with the exponential density distribution of the ejecta of Type Ia SN (Dwarkadas & Chevalier 1998), whereas the distribution of ejecta around core-collapse supernovae is better approximated by a power-law (Chevalier & Fransson 2003). Extrapolating the pre- and post-maximum fits we get a maximum bolometric luminosity of $L_{bol}^{max} = 5.6 \times 10^{43} \text{ ergs}^{-1}$, which is ~ 3 times more luminous than the Type Ia SN 1991T at maximum light (Contardo et al. 2000; Stritzinger et al. 2006). Assuming a bolometric correction of 50% at maximum, we find that SN 2005gj was ~ 1.5 times more luminous than SN 2002ic.

5.4. Optical spectroscopy

In Figure 11 we show a comparison of the spectra of SN 2005gj with spectra of SN 2002ic and SN 1997cy obtained at similar times after explosion. The spectra of SN 2005gj and SN 2002ic are very similar at all times. They are characterized by strong and broad

Hydrogen-Balmer lines $H\alpha$ and $H\beta$ in emission⁵ and a blue continuum at early times that becomes redder and increasingly dominated by absorption/emission P-cygni profiles from Fe-peak ions (e.g., Fe II, Fe III, Ni III, Si II, S II).

5.4.1. Classification

Benetti et al. (2006) proposed that SN 2002ic-like events are well explained by the core-collapse of a massive star in a dense medium, casting doubt in the previous classification of SN 2002ic as a Type Ia supernova. The authors found relatively good agreement at all times between the spectra of SN 2004aw (Taubenberger et al. 2006), a Type Ic supernova, and SN 2002ic.

We used the SuperNova IDentification code, SNID (Matheson et al. 2005; Miknaitis et al. 2007; Blondin & Tonry 2007), to find the spectra that best match SN 2005gj at different epochs. SNID cross-correlates an input spectrum with a library of supernovae spectra. In the library we included spectra of 5 normal SN Ia, two 1991T-like objects, two 1991bg-like objects, 4 broad-lined SN Ic (or hypernovae), and 3 normal SN Ic (including SN 2004aw), that were chosen to span a wide range of observed properties of SN Ia and SN Ic. In Table 9 we present the supernovae and the epochs of the spectra in the library. We fixed the redshift of SN 2005gj at $z = 0.0616$ and allowed for a range around the mean redshift of $\Delta z = 0.02$ to find cross-correlation peaks. The Balmer lines in emission were clipped from the input SN 2005gj spectra to avoid spurious cross-correlation signal with library spectra that contain emission lines from the host galaxy.

Figure 12 shows the spectra of SN 2005gj at four epochs and the library spectra with the highest cross-correlation significance from SNID. Type Ia supernovae spectra are a better match to SN 2005gj at most epochs, with 20 of the 26 (77%) epochs having best matched a type Ia spectrum (45%-91T, 45%-normal, 10%-91bg) and a similar fraction for the next-best matches. The broad-lined SN Ic 1997ef and 2002ap are the best matching spectra for 6 epochs, all of them between 26–46 days after explosion. We repeated the same procedure using five spectra of SN 2002ic obtained between 24–84 days after explosion (Hamuy et al. 2003). All the spectra of SN 2002ic are better matched with SN Ia, in contradiction with the results obtained by Benetti et al. (2006).

The continuum of SN 2005gj is well approximated at all times by the sum of a scaled spectrum of the overluminous Type Ia SN 1991T, at the same epoch after explosion as

⁵As shown in Figure 2, $H\gamma$ is also visible in the early spectra of SN 2005gj.

SN 2005gj, and a fourth order polynomial. A normal SN Ia does not fit as well as SN 1991T. This procedure is very similar to the fits to SN 2002ic (Hamuy et al. 2003) and SN 2005gj (Aldering et al. 2006) presented in previous studies. In Figure 13 we show examples of the spectra decomposition at four epochs. We excluded from the fit a region of $\pm 100 \text{ \AA}$ around the $H\alpha$ and $H\beta$ lines and obtained a good fit for the remainder of the spectrum.

5.4.2. Balmer lines

We analyzed the Balmer emission features in the spectra using the sum of two Gaussian components to model the line profiles. This decomposition gives much better fits for $H\alpha$ at all epochs than a single Gaussian and it is physically motivated (Chugai 1997a,b). The spectra of Type IIn SN show Balmer features with both a narrow and broad component that can be explained by radiation coming from different regions of the ejecta/CSM, whether it is direct emission from the shock-heated CSM (broad component) or emission from un-shocked gas photoionized by the SN radiation (narrow component). The $H\beta$ line is unresolved or only marginally resolved for most of the spectra. Therefore a single Gaussian component was used to fit the line profile. We used a third order polynomial to model the local continuum around each line that was included in the Gaussian fits. It is important to stress that at late times there is a broad Fe II feature intrinsic to the supernova spectrum in the region of $H\alpha$ (see spectra in Figure 13) that makes the definition of the continuum less reliable and may affect the line measurements.

The results of the Gaussian fits to the $H\alpha$ and $H\beta$ emission features, integrated fluxes and FWHM, are shown in Table 10 as a function of epoch of the spectra. We have excluded the two spectra with better resolution because they show P-Cygni profiles (see below). We used the flux calibrated spectra corrected to match the observed g , r magnitudes (as explained in § 5.1) and corrected for Galactic reddening in the line of sight. The FWHM of the Gaussian profiles listed in Table 10 were corrected by the resolution of the spectrographs (from Table 6). We do not present the values when the component is unresolved. The errors quoted for the integrated fluxes are obtained by adding in quadrature an estimate of 10% error assigned to the absolute flux calibration and the rms deviation of the Gaussian fits.

Figure 14 shows the evolution in time of the FWHM (top left panel), $H\alpha$ and $H\beta$ luminosities (top right and bottom left panels) and the Balmer decrement (bottom right panel). The FWHM of $H\alpha$ varies between $\sim 130 - 500 \text{ km s}^{-1}$ (narrow component) and $\sim 1200 - 3800 \text{ km s}^{-1}$ (broad component), with the broad component showing a slow increase in time. The FWHM of $H\beta$ varies between $\sim 470 - 1700 \text{ km s}^{-1}$ and does not show evident evolution. The luminosities of $H\alpha$ -narrow and $H\beta$ lines evolve in a similar fashion, increasing

at early times to peak at ~ 12 days with luminosities $6 - 6.5 \times 10^{40}$ ergs $^{-1}$, then they decay and stay roughly constant after 50 days. The evolution of H α -broad is similar during the first 50 days, peaking at 1.1×10^{41} ergs $^{-1}$, but it shows an increase at later times. Compared with the H α luminosities observed in SN 2002ic, both components are ~ 4 times more luminous.

The Balmer decrement, the ratio between H α (sum of narrow and broad components) and H β fluxes, stays approximately constant during the first 30 – 40 days (mean = 2.5 and rms = 0.5) and is consistent with the theoretical value in Case B recombination of H α /H β = 2.86 (Osterbrock 1989). At later times it shows a steady increase, reaching H α /H β $\sim 7 - 13$ at ~ 80 days. In Case B recombination a Balmer decrement H α /H β > 2.86 is usually interpreted as evidence for the presence of internal extinction in the host; however, the large values observed at late times would produce an Na I D interstellar absorption doublet easily detectable in the spectra, which is not observed (see also Aldering et al. (2006)), and the evolution in time is not expected. Aldering et al. (2006) proposed that the H level populations are in Case C recombination, where the optical depth in the H α line is high implying high densities and greater importance of collisional processes. In this scenario, the observed change in the Balmer decrement could indicate that collisional excitation becomes increasingly important at later times (Branch et al. 1981; Turatto, et al. 1993). SN 2002ic (Deng et al. 2004) and other SN IIn, like SN 1988Z (Aretxaga et al. 1999) and SN 1995G (Pastorello et al. 2002), have also shown large values of the Balmer decrement and therefore may have similar physical processes affecting the formation of the Balmer lines.

In Figure 15 we show the regions around H α and H β features in the best resolution spectra from ISIS and LDSS-3, obtained at 44 and 115 days after explosion, respectively. We clearly detect P-Cygni profiles in all these features, which indicates the presence of an outflow moving at ~ 150 -200 km s $^{-1}$; however, these measurements are limited by the resolution of the spectra between ~ 130 -180 km s $^{-1}$ (FWHM). After correcting for the resolution we obtain an outflow velocity of 60-70 km s $^{-1}$. The detection of P-Cygni-like absorption rules out an H II region in the line of sight that could be producing the narrow emission/absorption features; the line profiles are intrinsic to the SN. Aldering et al. (2006) detected P-Cygni profiles in He I, H α and H β , in a high resolution spectrum obtained with LRIS+Keck 71 days after the explosion. They derived a wind velocity of $v_w \approx 60$ km s $^{-1}$ consistent with our estimate. Kotak et al. (2004) also detected a P-Cygni profile in the a spectrum of SN 2002ic obtained 256 days after explosion.

5.4.3. Line identification near maximum

We used the parameterized resonance-scattering code SYNOW (Fisher et al. 1997; Fisher 2000) to identify the lines in the spectra obtained near maximum light of SN 2005gj. SYNOW is a fast supernova spectrum-synthesis code used for direct (empirical) analysis of supernova spectra, mainly to identify the lines, their formation velocities and optical depths. The code is based on simple assumptions: spherical symmetry, homologous expansion, a sharp photosphere that emits a black-body continuous spectrum, and line formation by resonance-scattering, treated in the Sobolev approximation. We have used the latest version of the code that includes a Gaussian distribution of optical depths.

Figure 16 shows the spectrum of SN 2005gj at 17 days after explosion (2 days before g maximum) and the best synthetic spectrum obtained with SYNOW. We also show for comparison the spectrum of SN 1991T obtained at -3 days with respect to the time of B maximum. The spectra have been locally normalized as in Jeffery et al. (2006). The synthetic spectrum has a black-body continuum temperature $T_{bb} = 11000$ K, photospheric velocity $v_{phot} = 10000$ km s $^{-1}$, and excitation temperature $T_{exc} = 10000$ K. We find a reasonably good match with the spectrum of SN 2005gj using the following lines/multiplets: Fe III $\lambda 4404$ and $\lambda 5129$, Si III $\lambda 4561$, Ni III, S II $\lambda 5468$ and $\lambda 5633$, and Si II $\lambda 6355$. These lines are characteristic of the overluminous and spectroscopically peculiar, Type Ia SN 1991T around maximum light with strong Fe III features and weak S II doublet and Si II (Jeffery et al. 1992; Mazzali et al. 1995; Fisher et al. 1999).

The main discrepancy between the SYNOW modeling of SN 2005gj and SN 1991T is in the optical depths of the lines. The fit to SN 2005gj needs unphysically small optical depths, approximately 1/10th of the values used for SN 1991T around maximum light. We interpret this as an effect of the *extra* continuum radiation that is added by the ejecta-CSM interaction, which is *veiling* (Branch et al. 2000) the supernova lines (e.g., Hamuy et al. 2003; Aldering et al. 2006). This interpretation is supported by the good agreement obtained from fitting the spectra of SN 2005gj using a simple polynomial continuum added to the spectra of SN 1991T at the same epochs after explosion (see Figure 13).

6. Discussion

We have presented extensive spectroscopy and optical/NIR photometry of SN 2005gj obtained by the SDSS-II and CSP supernova groups during the first ~ 150 days after explosion, and also an X-ray observation at 74 days that gives an upper limit on the X-ray luminosity. We have shown the remarkable similarity in spectroscopic and photometric properties be-

tween SN 2005gj and SN 2002ic, which is thought to be the first clear case of a thermonuclear supernova explosion embedded in a dense CSM. The observational properties of SN 2005gj support this interpretation, they are summarized as follows:

- Spectroscopic evidence for a shock propagating into an Hydrogen-rich medium close to the site of the explosion inferred from the presence of Balmer lines with narrow ($\text{FWHM} \sim 200 - 500 \text{ km s}^{-1}$) and broad ($\text{FWHM} \sim 1500 - 3000 \text{ km s}^{-1}$) components at all times. The Balmer lines show P-Cygni profiles in the highest resolution spectra obtained at 44 and 115 days after explosion, these detections show the presence of a slow ($\sim 100 \text{ km s}^{-1}$) moving outflow. Both observations support the interpretation of the supernova ejecta interacting with a dense circumstellar material.
- Spectrum evolves from a very blue continuum (13000 K black-body) similar to SN IIn at ~ 7 days after explosion to a redder continuum at later times with P-Cygni absorption/emission profiles. The strongest lines present around maximum are identified with singly and doubly ionized iron-peak elements (especially strong Fe III, weak S II and Si II) and the spectra are well matched by the overluminous Type Ia SN 1991T *diluted* with a polynomial continuum at similar times after explosion.
- Very luminous and slowly declining bolometric light curve. The linear decay in luminosity after peak ($\sim 0.014 \text{ mag day}^{-1}$) suggests an exponential density distribution of the ejecta, which is consistent with the ejecta-density profiles obtained from simulations of SN Ia.

The data presented here on SN 2005gj makes the interpretation of 2002ic-like events as thermonuclear supernovae in a dense CSM, initially proposed by Hamuy et al. (2003), stronger. In contrast with Benetti et al. (2006), we find that the overall shape of the spectra of SN 2005gj are more consistent with spectra of SN Ia at different epochs. Specifically, Type Ic SNe usually do not show the S II doublet at $\sim 5500 \text{ \AA}$ around maximum light; in fact SN 2004aw shows only two very weak notches at the wavelengths of S II near maximum (Taubenberger et al. 2006). This is one of the identifying features in SN Ia spectra, also present in the overluminous SN 1991T (Phillips et al. 1992). In the spectrum of SN 2005gj obtained at 17 days (see Figure 16) we detect a weak double absorption that we identify with S II, that is much stronger in the spectrum of SN 2002ic around maximum light. We can see on the top of Figure 11 that the spectrum of SN 2002ic obtained 24 days after explosion clearly shows this feature. Other conspicuous features observed in SN 2005gj and SN 2002ic around maximum are Fe III and Si II. These features are present in SN 1991T, but Fe III is not observed and Si II is generally weaker in SN Ic.

SN 2005gj has stronger ejecta-CSM interaction than SN 2002ic. The peak bolometric luminosity is ~ 1.5 times brighter and the broad and narrow components of $H\alpha$ are ~ 4 times more luminous in SN 2005gj. The fact that the SN 1991T features are weaker in SN 2005gj compared with SN 2002ic at similar epochs is consistent with this interpretation, because the supernova features are more *diluted* by the stronger continuum. The absence of evidence for a secondary maximum in SN 2005gj, whereas the i band light curve of SN 2002ic does show a hint of such a feature, is likewise consistent with the ejecta-CSM interaction in SN 2005gj having been stronger than in SN 2002ic.

6.1. Structure of the CSM

The circumstellar interaction of core-collapse supernovae with a circumstellar medium has been studied in detail in the literature (see Chevalier & Fransson (2003) for a review). When the fast moving ejecta encounters the approximately stationary CSM, a forward shock moving into the CSM (also called circumstellar shock) and a reverse shock develops. The fast-moving shockwave implies large post-shock temperatures, therefore radiating energy in the X-ray regime. The density distribution of the ejecta and the CSM can be well described by power-laws in radius, which leads to a set of self-similar analytical solutions for the evolution of the shock radius in time (Chevalier 1982). The physics of the ejecta-CSM interaction in the case of thermonuclear supernovae is basically the same, the main difference is in the distribution of the ejected material which follows an exponential function in velocity (Dwarkadas & Chevalier 1998). In this case the solutions are no longer analytic. The density profile of the shocked region is different in the case of exponential ejecta expanding into a constant density medium, but the similarity increases for expansion into a wind profile whose density decreases as $\propto r^{-2}$.

A simple self-similar model of a SN shock expanding into a medium with a power-law density decline, as suggested for core-collapse SNe by Chevalier (1982), is ruled out for this object by several observations: the exponential decrease in luminosity, suggesting an exponential ejecta density profile; the strange behavior of the broad and narrow $H\alpha$ components; and the decrease in the blackbody radius at later times. Detailed calculations of the SN-CSM interaction would require highly detailed hydrodynamic modeling, which are beyond the scope of this paper. Instead herein we focus on trying to explain the basic features of SN-CSM interaction as deduced from the observational data.

The initial velocity of a SN shock wave as it breaks out from the surface is at least of the order of $2 \times 10^4 \text{ km s}^{-1}$. The broad $H\alpha$ velocities that are seen in the first week or so are of the order of 1500 km s^{-1} , and increase to more than twice this value after ~ 50 days. These

velocities are almost an order of magnitude smaller than expected SN blast wave velocities in the early stages, and a factor of few smaller even after ~ 50 days. Furthermore, the SN shock velocity would be expected to gradually decrease as the shock moves outwards, whereas the $H\alpha$ profile actually indicates an increasing velocity after ~ 50 days.

For these reasons, we suggest that the broad $H\alpha$ lines do not indicate the SN velocity. Instead, we put forward a scenario of a shock expanding into a two-component ambient medium: a low density wind in which are embedded high-density clumps. In this picture, there should theoretically exist three different velocity components: a broad velocity component, which is not easily seen in this case, and is related to the velocity of the blast wave itself; an intermediate velocity component, which is what we have referred to as the broad $H\alpha$ and is related to the velocity of the shock driven into the clumped material; and a narrow velocity component, which may be related to the narrow $H\alpha$ and is representative of the velocity of the ambient medium. This scenario is like the scenario put forward by (Chugai & Danziger 1994) to explain the origin of the broad, intermediate and narrow line components in SN 1988Z. The large $H\alpha$ luminosity of SN 2005gj at late times is very similar to that seen in other Type II In SNe, and is especially large considering that this was a Type Ia. However, there are significant differences. We do not see a really broad line component representative of the SN velocity, although there are some suggestions that this may be appearing at late times. In particular, the $H\alpha$ profile of the spectrum obtained at ~ 150 days is better fitted by three components, including a very broad component with $\text{FWHM} \approx 7000 \text{ km s}^{-1}$.

Our scenario envisions the Type Ia SN shock wave expanding in a clumped medium presumably formed by mass-loss from a companion star. The broad component is not easily visible in $H\alpha$ initially because the forward shock is not radiative. The density of the clumps is much higher than that of the interclump (ambient) medium. When the SN shock wave interacts with a dense cloud or clump, it drives a strong shock into the clump. A reflected shock is driven back into the expanding ejecta (Klein et al. 1994). Assuming pressure equilibrium, the ratio of the velocity of the clump shock to that of the blast wave is inversely proportional to the square-root of the ratio of the clump density to that of the interclump medium. The optical emission arises from behind the clump shock, probably by reprocessing of the X-ray emission.

In this model, the intermediate component represents the velocity of the clump shock, which is probably radiative. If we assume that the initial velocity of the SN shock wave is $\sim 20000 \text{ km s}^{-1}$ and the broad $H\alpha$ emission velocity is $\sim 1500 \text{ km s}^{-1}$, then the ratio of velocities is 13 – 14. This indicates that the clump density is about 14^2 , or ~ 200 times the interclump density. Note that the optical emission, which goes as density squared, will then

be 200^2 times, or about 40,000 times greater compared to that from the interclump medium. This is consistent with the fact that no broad line emission is seen from the interclump medium. If the initial velocity is much higher, as is conceivable, the clump density could be up to $\sim 50\%$ higher, and the ratio between the emission from the dense clumps and interclump medium even larger.

What value of the clump density is suggested? A shock wave traveling at 1500 km s^{-1} would be radiative if it were expanding in a medium whose density is greater than $\sim 10^6 \text{ cm}^{-3}$, whereas a 2500 km s^{-1} shock would require minimum densities of the order of 10^7 cm^{-3} (Draine & McKee 1993) in order to be radiative. The CSM density, being two orders of magnitude smaller, would then to be $\gtrsim 10^4 \text{ cm}^{-3}$. These are just minimum values, and it is conceivable that the actual clump density is much higher. This result is consistent with the conclusion of Aldering et al. (2006).

The observations show that the broad $\text{H}\alpha$ width increases after 50 days, suggesting an increase in the clump shock velocity at later times, which could perhaps be due to a decrease in the clump density. Conversely, however, the luminosity of the $\text{H}\alpha$ also increases, suggesting an increase in the electron density. At the same time, we would expect the SN shock to be decreasing in velocity as it continues its outwards expansion.

We suggest that the way to reconcile these observations is a scenario in which the density within the clump medium starts out higher than 10^8 cm^{-3} , probably as high as 10^{10} cm^{-3} in the first few days, and decreases gradually outwards. The almost constant behavior of the FWHM of the broad $\text{H}\alpha$ suggests that the density profile of the ambient medium is flatter than r^{-2} . Since we want the clump shock to be radiative even when the shock velocity is almost 3000 km s^{-1} , this suggest that the density at ~ 150 days is greater than about 10^7 cm^{-3} . And since the density is decreasing outwards, we infer that the density close in is even larger. Over the entire period of observations the clump density is large enough that the shock driven into these clumps is always radiative. The density of the ambient medium is two orders of magnitude smaller, as discussed above. The high bolometric luminosity is consistent with these values.

For the first ~ 50 days the $\text{H}\alpha$ emission arises only from the radiative shock driven into the dense clumps. However, by ~ 50 days the SN forward shock, which is decreasing in velocity, enters the radiative regime, and the cooling shell of material begins to contribute to the $\text{H}\alpha$ luminosity. The velocity of the SN shock is quite large, and its contribution initially is not a large fraction of the total $\text{H}\alpha$ luminosity. But as it expands outwards, its velocity decreases and the shock becomes more radiative, and the contribution to the total $\text{H}\alpha$ luminosity increases, more than compensating for the decreasing density. If this conclusion is correct, then we would expect that a broad velocity component would be visible

in the $H\alpha$ spectra, whose intensity would gradually increase with time even as the FWHM decreases. Although the underlying supernova contamination makes it hard to isolate a broad component, it is suggestive that by day ~ 150 the spectrum is best fit by a third, much broader component of the velocity, thus providing support for this line of reasoning.

Finally, in this model the narrow line emission arises from the unshocked slowly expanding ambient material, presumably the outflow that we find expanding at $\sim 60 \text{ km s}^{-1}$. We note that although the width of the narrow line $H\alpha$ emission as listed is higher, it is still unresolved, and it is possible that within the limits of resolution the narrow line component and outflow velocity are indeed the same.

To summarize, in this model the Type Ia SN expands in a clumped ambient medium, with the clump density about ~ 200 times that of the surrounding medium close in to the star, and decreasing as we go outwards. The $H\alpha$ emission initially arises mainly from the shock driven into the dense clumps. The SN shock propagating into the interclump medium begins to enter the radiative regime around day 50, and its contribution to the $H\alpha$ emission gradually increases beyond that coming from the clumped medium, leading to the gradual rise in the $H\alpha$ emission. We note that several features of this model are similar to the model presented by Chugai et al. (2004) for SN 2002ic, thus further supporting the similarity between the two supernovae.

The upper limit on the X-ray luminosity obtained at 74 days after the explosion can put a constrain on the mass loss rate from the precursor or companion (e.g., Immler et al. 2006). Assuming that the X-ray luminosity is dominated by emission from the reverse shock we obtain $\dot{M} \lesssim 2 \times 10^{-4} \text{ M}_{\odot} \text{ yr}^{-1}$ (2σ) using Equation 3.10 in Fransson et al. (1996). This value has to be taken as an approximate estimate because we are making several assumptions about the physical properties of the ejecta-CSM interaction that should be calculated using detailed hydrodynamical simulations: a constant velocity of the shock, $V_{sh} \approx 8000 \text{ km s}^{-1}$; a solar composition of the CSM material; an electron temperature at the reverse shock of $T_e = 10^7 \text{ K}$, which comes from the modeling of SN 2002ic (Nomoto et al. 2005); a flat density profile of the CSM, $\rho \propto r^{-2}$; and a power-law ejecta density profile with index $n = 7$ (Nomoto et al. 1984).

We can also estimate a mass loss rate from the companion using the density of the ambient medium ($n \sim 10^8 \text{ cm}^{-3}$), the initial optical radius of the CSM ($R \approx 10^{15} \text{ cm}$), and the velocity of the wind: $\dot{M} = 4\pi R^2 v \rho$, this is assuming a flat density profile for the CSM. We obtain: $\dot{M} \approx 2 \times 10^{-4} \text{ M}_{\odot} \text{ yr}^{-1}$, which is in agreement with the 2σ upper limit calculated from the X-ray luminosity.

The presence of Balmer lines in emission in the first spectrum obtained 6.6 days af-

ter explosion shows that the ejecta started to interact with the CSM at an earlier epoch (Aldering et al. 2006). Extrapolating linearly to zero flux the early increase of $H\alpha$ and $H\beta$ fluxes we find that the ejecta-CSM interaction started 3 ± 1 days after explosion, which gives an internal radius of the CSM $R_i \approx 1.1 \times 10^{15}$ cm. The outer radius of the CSM can be estimated assuming a constant velocity of the shock of $V_{sh} \approx 8000$ km s $^{-1}$ over the first year. We detect $H\alpha$ in emission in a spectrum obtained at 368 days after explosion, which will be presented elsewhere, putting a lower limit on the outer radius of the CSM, $R_o \gtrsim 3 \times 10^{16}$ cm. This is also consistent with a Type Ia SN with an exponential ejecta density profile expanding outwards in a medium of average density $\gtrsim 10^7$ cm $^{-3}$.

In the interpretation above we assume that the broad component of the Hydrogen Balmer lines originate in the dense clumps, while the narrow component arises from the photoionized un-shocked gas. However, Thompson scattering of the lines has been considered as an alternative mechanism that can explain relatively well the symmetric line profiles of SN 2002ic (Wang et al. 2004) and SN 2005gj (Aldering et al. 2006). In this scenario, both components would arise from a single high density region. The total mass of hydrogen in the emitting region would be $M_H \approx 2 \times 10^{-2} (10^{10}/n_e) M_\odot$, where n_e is the average electron density in the emitting zone, as calculated from the luminosity of the $H\alpha$ line at maximum using the Case B recombination coefficient. The electron density must be sufficiently high, $n_e \approx 10^{10}$ cm $^{-3}$, to be consistent with the line ratios of He lines observed in the spectra (Aldering et al. 2006), and a high electron density would explain the non-detection in X-ray and radio (Soderberg & Frail 2005). However, it is unlikely that this model would be able to explain the initial constancy and then rise of the broad $H\alpha$ luminosity.

6.2. Rates, hosts galaxies and possible progenitors of SN 2002ic-like supernovae

The SDSS-II Supernova Survey has a well understood discovery efficiency of SN Ia at low redshift ($z \lesssim 0.1$), which allows us to obtain an accurate supernova rate measurement controlling systematic errors (Dilday et al. 2007). In the fall 2005 season there were a total of 16 spectroscopically confirmed SN Ia (including 1991T-like and 1991bg-like objects) at $z < 0.12$, one photometric identification, and the spectroscopically confirmed peculiar events: SN 2005hk (Phillips et al. 2007) and SN 2005gj. Since the detection efficiency of 2002ic-like objects has not been carefully modeled, we can only put a lower limit on the fraction of these events. The spectroscopic confirmation of one object at $z < 0.12$ puts a lower limit of $5^{+7}_{-4}\%$ (68% confidence) in the fraction of 2002ic-like events among SN Ia at low redshift. From the previously known (2002ic) and probable events (1997cy and 1999E) the estimated fraction

is $\sim 1\%$ of SN Ia discovered between 1997 and 2002, which is consistent with our limit.

In the fall of 2006 we obtained the spectrum of a slowly declining supernova that was discovered in 2005, but did not have a spectroscopic classification, SN 7017⁶. To our surprise, the late spectrum of SN 7017 resembles that of SN 2005gj one year after explosion and the early photometry also shows similarities which lead us to classify it as the highest redshift SN 2002ic-like object observed to date, at $z = 0.27$ (Prieto et al. 2007, in preparation). Considering SN 7017 in the spectroscopically confirmed sample of SN Ia during the 2005 season, a total of 129 SNe at $z \lesssim 0.42$, we have that 2/130 (1.5%) are SN 2002ic like objects, which is consistent with the low limit on the fraction at low redshift estimated before. However, this fraction has to be taken with extreme care and probably does not reflect the *true* fraction. This is because the discovery efficiency of SN Ia declines as a function of redshift and the total number of spectroscopically confirmed SN Ia does not include SNe with good Ia-like light curves that were not spectroscopically classified. A more careful study of the rates of SN 2005gj-like supernovae in the SDSS-II is planned for a future publication.

The host galaxies of supernovae can provide important clues about their progenitors. The host of SN 2005gj is a very blue, low-luminosity dwarf ($M_B \approx -17$), and has an irregular morphology with no well defined core. Aldering et al. (2006) combined the SDSS photometry with UV imaging from GALEX to construct an SED of the galaxy. They constrained the metallicity to $Z < 0.3 Z_\odot$, with a burst of star formation ~ 200 Myr ago. SN 2002ic has a late type (Sbc) spiral host with a well defined core. The host of SN 1997cy is also a blue, low-luminosity ($M_V \approx -18.2$), and low surface brightness dwarf irregular galaxy (Germany et al. 2000). GALEX has imaged the positions of SN 1997cy, 2002ic and 2005gj, and their hosts galaxies are all detected in the Near-UV (NUV) band. Their absolute magnitudes in the NUV (AB magnitudes) are between -16.6 (SN 2005gj) and -17.3 (SN 1997cy and 2002ic). They are low-luminosity late type galaxies, $\sim 1 - 1.7$ magnitudes fainter than L^* galaxies observed by GALEX at redshift $z < 0.1$ (Wyder et al. 2005). The host galaxy of SN 1999E is a late spiral with a nuclear starburst first observed by the IRAS satellite (Allen et al. 1991). From 2MASS photometry, its absolute magnitude is 1 mag brighter than an L^* galaxy in the K -band (Kochanek et al. 2001). SN 7017 at redshift $z = 0.27$, has a blue, dwarf-like host galaxy with absolute magnitude in B of -17.9 .

The host galaxies of the five SN 2002ic-like objects known share some common properties: they are late type galaxies, irregulars and late spirals, most likely with recent star formation. Four of the host galaxies have low luminosities, similar to the Magellanic clouds,

⁶This is the internal name given by the SDSS-II Collaboration. It was not announced in an IAU circular because of the late spectroscopic classification.

which indicates they are low metallicity systems. For example, a dwarf galaxy with intrinsic luminosity $M_B = -18$ has an Oxygen abundance of $12 + \log(\text{O}/\text{H}) \approx 8.4$ (van Zee et al. 2006), which corresponds to 1/3 the solar Oxygen abundance (Delahaye & Pinsonneault 2006). On the other hand, the host galaxy of SN 1999E has a K -band luminosity, that when converted to metallicity using the luminosity-metallicity relationship derived by Salzer et al. (2005), makes it consistent with the solar value. The host luminosities are only an approximate indicator of their metallicities, therefore spectra of the hosts are needed to infer the metallicities and star formation rates (SFRs) of these galaxies. However, it is interesting to note that the range of host galaxy properties of SN 2002ic-like events seem to be inconsistent with the host galaxies of GRBs associated with supernovae (Stanek et al. 2006) and broad-lined type Ib/c SNe (Modjaz et al. 2007).

Type Ia supernovae are observed in all types of galaxies. There is a well established correlation between the morphology of their host galaxies and the peak luminosity of the SNe: brighter supernovae (1991T-like) tend to explode in late type spirals and irregulars with recent star formation, while intrinsically fainter events (1991bg-like) are observed mainly in early type galaxies with an old stellar population (Hamuy et al. 1995, 1996a; Branch et al. 1996; Hamuy et al. 2000; Gallagher et al. 2005). This environmental effect and observations of the local supernovae rate as a function of host galaxy properties (Cappellaro et al. 1999; Mannucci et al. 2005), motivated Scannapieco & Bildsten (2005) to parametrize the delay time distribution, time between star formation and the appearance of SNe, and the rates with a two-component model having a piece proportional to the SFR of the host galaxy (or *prompt*, they explode $\sim \text{few} \times 10^8$ yr after an episode of star formation), and a second piece proportional to the total stellar mass (*delayed* component, they explode on scales of a few Gyr after the onset of star formation). The difference in age of the stellar populations of these subclasses suggests that the progenitors may also be different: *prompt* SN Ia would come from more massive progenitors. The host galaxies of all five SN 2002ic-like events known are broadly consistent with the properties of the hosts of *prompt* SN Ia, which suggest a real association given that the best studied SN IIa to date, SN 2002ic and SN 2005gj, have spectral characteristics similar to 1991T-like events.

Several progenitors have been discussed in the literature for SN 2002ic and SN 2005gj. Livio & Riess (2003) proposed that SN 2002ic is a rare case of a double-degenerate binary system, a white dwarf (WD) and the core of an AGB star spiraling-in through gravitational wave losses, in which the explosion occurs during or immediately after the common-envelope phase (a few hundred to a few thousand years of duration). The difference in line strengths of the Balmer emission lines observed for SN 2002ic and SN 2005gj makes this scenario unlikely. Also, as Aldering et al. (2006) points out, in both SN 2002ic and SN 2005gj the mass loss stopped only a few years before explosion, which is too short compared with the

timescale for gravitational wave radiation to produce the merger of the core and the WD.

Another possible progenitor initially proposed by Hamuy et al. (2003) and favored by the models of Chugai et al. (2004), is the explosion of the Chandrasekhar-mass Carbon-Oxygen core of a massive AGB star in a degenerate medium, a supernova Type 1.5 (Iben & Renzini 1983), where the dense Hydrogen-rich CSM would come from the outer layers of the AGB. In order for the core to grow to the Chandrasekhar mass, the radiatively driven winds from the AGB have to be weak enough, a condition that is only met in a very low-metallicity environment like the Galactic halo (Zijlstra 2004). At face value, the range of host galaxy metallicities for SN 2002ic-like events inferred from the luminosity-metallicity relation does not support the SN 1.5 scenario, although admittedly these are average metallicities and do not tell us the actual range of metallicities of the progenitors.

Han & Podsiadlowski (2006) proposed that SN 2002ic could be produced through the “super-soft channel”, the most common single-degenerate model for the progenitors of SN Ia. In this scenario the white dwarf is accreting material from a main sequence, or slightly evolved, relatively massive companion ($\sim 3 M_{\odot}$) and experiences a delayed dynamical instability that leads to a large amount of mass-loss from the system in the last few $\times 10^4$ yr before the explosion. Aldering et al. (2006) notes that the estimated main-sequence mass of the progenitor of SN 2005gj of $\sim 2 M_{\odot}$, calculated using the age of the starburst of its host galaxy, is consistent with the Han & Podsiadlowski (2006) model. Also, the predicted fraction of SN Ia that would be produced through the “delayed dynamical” channel is 0.1-1%, consistent with the limits we have obtain from the detection of SN 2005gj in the SDSS-II Survey.

In general terms, the progenitor model proposed by Han & Podsiadlowski (2006) successfully reproduces the observational properties of SN 2002ic and SN 2005gj. However, it is still very early in the study of this new sub-class of SN Ia. It would be interesting to see in the near future the results of theoretical modeling exploring other single degenerate configurations (e.g., AGB donor) and detailed hydrodynamical modeling of the ejecta-CSM interaction of SN 2005gj using the observations of the early photometric and spectroscopic evolution presented in this work.

We are grateful for the assistance of the staffs at the many observatories (APO, MDM, LCO, ESO, La Palma) where data for this paper were obtained. We would like to thank K. Z. Stanek and R. Pogee for helpful discussions, and L. Watson for carefully reading an earlier version of this paper. We also thank S. Taubenberger for making the electronic form of the SN 2004aw data available, and S. Blondin for allowing us to use the SNID code before

its public release. We wish to thank H. Tananbaum and the Chandra Observatory for the generous allotment of Director’s Discretionary Time. VVD research is supported by award # AST-0319261 from the National Science Foundation, and by NASA through grant # HST-AR-10649 awarded by the Space Science Telescope Institute. MH acknowledges support from Centro de Astrofísica FONDAP 15010003, Proyecto Fondecyt 1060808, and Proyecto P06-045-F from Iniciativa Científica Milenio. DP gratefully acknowledges the support provided by NASA through Chandra Postdoctoral Fellowship grant PF4-50035 awarded by the Chandra X-Ray Center, which is operated by the Smithsonian Astrophysical Observatory for NASA under contract NAS8-0306. This paper is based upon CSP observations supported by the NSF under grant AST 0306969. Use was also made of the CfA Supernova Archive, which is funded in part by the NSF through grant AST 0606772.

Funding for the SDSS and SDSS-II has been provided by the Alfred P. Sloan Foundation, the Participating Institutions, the National Science Foundation (NSF), the U.S. Department of Energy, the National Aeronautics and Space Administration, the Japanese Monbukagakusho, the Max Planck Society, and the Higher Education Funding Council for England.

The SDSS is managed by the Astrophysical Research Consortium for the Participating Institutions. The Participating Institutions are the American Museum of Natural History, Astrophysical Institute Potsdam, University of Basel, Cambridge University, Case Western Reserve University, University of Chicago, Drexel University, Fermilab, the Institute for Advanced Study, the Japan Participation Group, Johns Hopkins University, the Joint Institute for Nuclear Astrophysics, the Kavli Institute for Particle Astrophysics and Cosmology, the Korean Scientist Group, the Chinese Academy of Sciences (LAMOST), Los Alamos National Laboratory, the Max-Planck-Institute for Astronomy (MPIA), the Max-Planck-Institute for Astrophysics (MPA), New Mexico State University, Ohio State University, University of Pittsburgh, University of Portsmouth, Princeton University, the United States Naval Observatory, and the University of Washington.

REFERENCES

- Aldering, G., et al. 2006, ArXiv Astrophysics e-prints
- Allen, D. A., et al. 1991, MNRAS, 248, 528
- Aretxaga, I., et al. 1999, MNRAS, 309, 343
- Arnett, W. D. 1982, ApJ, 253, 785
- Astier, P., et al. 2006, A&A, 447, 31
- Barentine, J., et al. 2005, Central Bureau Electronic Telegrams, 247, 1 (2005). Edited by Green, D. W. E., 247
- Benetti, S., et al. 2006, ApJ, 653, L129
- Blondin, S. & Tonry, J. L. 2007, ApJ, in press
- Branch, D., et al. 1981, ApJ, 244, 780
- Branch, D., et al. 2003, AJ, 126, 1489
- Branch, D., et al. 2000, PASP, 112, 217
- Branch, D., Romanishin, W., & Baron, E. 1996, ApJ, 465, 73
- Cappellaro, E., Evans, R., & Turatto, M. 1999, A&A, 351, 459
- Cardelli, J. A., Clayton, G. C., & Mathis, J. S. 1989, ApJ, 345, 245
- Chevalier, R. A. 1982, ApJ, 258, 790
- Chevalier, R. A. & Fransson, C. 1994, ApJ, 420, 268
- Chevalier, R. A. & Fransson, C. 2003, in LNP Vol. 598: Supernovae and Gamma-Ray Bursters, ed. K. Weiler, 171–194
- Chugai, N. N. 1997a, Ap&SS, 252, 225
- . 1997b, Astronomy Reports, 41, 672
- Chugai, N. N., Chevalier, R. A., & Lundqvist, P. 2004, MNRAS, 355, 627
- Chugai, N. N. & Danziger, I. J. 1994, MNRAS, 268, 173
- Contardo, G., Leibundgut, B., & Vacca, W. D. 2000, A&A, 359, 876

- Delahaye, F. & Pinsonneault, M. H. 2006, *ApJ*, 649, 529
- Deng, J., Kawabata, K. S., Ohyama, Y., et al. 2004, *ApJ*, 605, L37
- Di Carlo, E., et al. 2002, *ApJ*, 573, 144
- Dilday, B., et. al. 2007, in preparation
- Draine, B. T. & McKee, C. F. 1993, *ARA&A*, 31, 373
- Dwarkadas, V. V. & Chevalier, R. A. 1998, *ApJ*, 497, 807
- Fisher, A., et al. 1999, *MNRAS*, 304, 67
- Fisher, A., et al. 1997, *ApJ*, 481, L89+
- Fisher, A. K. 2000, PhD thesis, AA(THE UNIVERSITY OF OKLAHOMA)
- Fransson, C., Lundqvist, P., & Chevalier, R. A. 1996, *ApJ*, 461, 993
- Freedman, W. L., et al. 2001, *ApJ*, 553, 47
- Frieman, J. A., et. al. 2007, submitted to *AJ*
- Fukugita, M., et al. 1996, *AJ*, 111, 1748
- Gal-Yam, A., et al. 2006, *ArXiv Astrophysics e-prints*
- Gal-Yam, A., Ofek, E. O., & Shemmer, O. 2002, *MNRAS*, 332, L73
- Gallagher, J. S., et al. 2005, *ApJ*, 634, 210
- Garavini, G., et al. 2004, *AJ*, 128, 387
- Garnavich, P. M., et al. 2004, *ApJ*, 613, 1120
- Germany, L. M., et al. 2000, *ApJ*, 533, 320
- Gunn, J. E., et al. 1998, *AJ*, 116, 3040
- Gunn, J. E., et al. 2006, *AJ*, 131, 2332
- Hamuy, M., et al. 1993, *PASP*, 105, 787
- Hamuy, M., et al. 1995, *AJ*, 109, 1
- Hamuy, M., et al. 1996a, *AJ*, 112, 2391

- . 1996b, *AJ*, 112, 2398
- Hamuy et al. 2000, *AJ*, 120, 1479
- Hamuy, M., et al. 2002, *AJ*, 124, 417
- Hamuy, M., et al. 2003, *Nature*, 424
- Hamuy, M., et al. 2006, *PASP*, 118, 2
- Han, Z. & Podsiadlowski, P. 2006, *MNRAS*, 368, 1095
- Hogg, D. W., et al. 2001, *AJ*, 122, 2129
- Holtzman, J., et. al. 2007, in preparation
- Iben, Jr., I. & Renzini, A. 1983, *ARA&A*, 21, 271
- Immler et al. 2006, *ApJ*, 648, L119
- Immler, S., Petre, R., & Brown, P. 2005, *IAU Circ.*, 8633, 2
- Ivezić, Ž., et al. 2007, *ArXiv Astrophysics e-prints*
- Ivezić, Ž., et al. 2004, *Astronomische Nachrichten*, 325, 583
- Iwamoto, K., et al. 2000, *ApJ*, 534, 660
- Jeffery, D. J., et al. 2006, *ArXiv Astrophysics e-prints*
- Jeffery, D. J., et al. 1992, *ApJ*, 397, 304
- Jha, S., et al. 1999, *ApJS*, 125, 73
- Kirshner, R. P., et al. 1993, *ApJ*, 415, 589
- Klein, R. I., McKee, C. F., & Colella, P. 1994, *ApJ*, 420, 213
- Kochanek, C. S., et al. 2001, *ApJ*, 560, 566
- Kotak, R., et al. 2004, *MNRAS*, 354, L13
- Kraft, R. P., Burrows, D. N., & Nousek, J. A. 1991, *ApJ*, 374, 344
- Krisciunas, K., Phillips, M. M., & Suntzeff, N. B. 2004, *ApJ*, 602, L81
- Leibundgut, B., et al. 1991, *ApJ*, 371, L23

- Leibundgut, B., et al. 1993, *AJ*, 105, 301
- Livio, M. & Riess, A. G. 2003, *ApJ*, 594, L93
- Lupton, R. H., Gunn, J. E., & Szalay, A. S. 1999, *AJ*, 118, 1406
- Mannucci, F., et al. 2005, *A&A*, 433, 807
- Martini, P., et al. 2004, in *Ground-based Instrumentation for Astronomy*. Edited by Alan F. M. Moorwood and Iye Masanori. *Proceedings of the SPIE*, Volume 5492, pp. 1653–1660 (2004)., ed. A. F. M. Moorwood & M. Iye, 1653–1660
- Matheson, T., et al. 2005, *AJ*, 129, 2352
- Mazzali, P. A., Danziger, I. J., & Turatto, M. 1995, *A&A*, 297, 509
- Miknaitis, G., et al.(2007), *ArXiv Astrophysics e-prints*
- Millard, J., et al. 1999, *ApJ*, 527, 746
- Modjaz, M., et al. 2007, *ArXiv Astrophysics e-prints*
- Modjaz, M., et al. 2006, *ApJ*, 645, L21
- Morgan, C. W., et al. 2005, *AJ*, 129, 2504
- Nomoto, K., Thielemann, F.-K., & Yokoi, K. 1984, *ApJ*, 286, 644
- Nomoto, K., et al. 2005, in *ASP Conf. Ser. 342: 1604-2004: Supernovae as Cosmological Lighthouses*, ed. M. Turatto, S. Benetti, L. Zampieri, & W. Shea, 105–+
- Nugent, P., Kim, A., & Perlmutter, S. 2002, *PASP*, 114, 803
- Oke, J. B., & Gunn, J. E. 1983, *ApJ*, 266, 713
- Osterbrock, D. E. 1989, *Astrophysics of gaseous nebulae and active galactic nuclei* (Research supported by the University of California, John Simon Guggenheim Memorial Foundation, University of Minnesota, et al. Mill Valley, CA, University Science Books, 1989, 422 p.
- Pastorello, A., et al. 2002, *MNRAS*, 333, 27
- Patat, F., et al. 2001, *ApJ*, 555, 900
- Perlmutter, S., et al. 1999, *ApJ*, 517, 565

- Persson, S. E., et al. 2002, *AJ*, 124, 619
- Phillips, M. M., et al. 1992, *AJ*, 103, 1632
- Phillips, M. M. 1993, *ApJ*, 413, L105
- Phillips, M. M., et al. 2007, *PASP*, 119, 360
- Pier, J. R., et al. 2003, *AJ*, 125, 1559
- Prieto, J., et al. 2005, *IAU Circ.*, 8633
- Riess, A. G., et al. 1998, *AJ*, 116, 1009
- Riess, A. G., et al. 2004, *ApJ*, 607, 665
- Riess, A. G., et al. 2005, *ApJ*, 627, 579
- Riess, A. G., et al. 2006, *ArXiv Astrophysics e-prints*
- Rigon, L., et al. 2003, *MNRAS*, 340, 191
- Salzer, J. J., et al. 2005, *ApJ*, 624, 661
- Scannapieco, E. & Bildsten, L. 2005, *ApJ*, 629, L85
- Schlegel, E. M. 1990, *MNRAS*, 244
- Schlegel, D. J., Finkbeiner, D. P., & Davis, M. 1998, *ApJ*, 500, 525
- Schmidt, B. P., et al. 1994, *ApJ*, 434, L19
- Smith, J. A., et al. 2002, *AJ*, 123
- Soderberg, A. M. & Frail, D. A. 2005, *The Astronomer’s Telegram*, 663, 1
- Spergel, D. N., et al. 2006, *ArXiv Astrophysics e-prints*
- Stanek, K. Z., et al. 2006, *Acta Astronomica*, 56, 333
- Stritzinger, M., et al. 2006, *A&A*, 460, 793
- Taubenberger, S., et al.(2006), *MNRAS*, 371, 1459
- Tucker, D. L., et al. 2006, *Astronomische Nachrichten*, 327, 821
- Turatto, M., et al. 1993, *MNRAS*, 262, 128

- Turatto, M., et al. 2000, ApJ, 534, L57
- van Zee, L., Skillman, E. D., & Haynes, M. P. 2006, ApJ, 637, 269
- Wang, L., et al. 2004, ApJ, 604, L53
- Wood-Vasey, W. M., et al. 2007, ArXiv Astrophysics e-prints
- Wood-Vasey, W. M., Wang, L., & Aldering, G. 2004, ApJ, 616, 339
- Wyder, T. K., et al. 2005, ApJ, 619, L15
- York, D. G., et al. 2000, AJ, 120, 1579
- Zijlstra, A. A. 2004, MNRAS, 348, L23

Table 1. SDSS *ugriz* and CSP *u'g'r'i'* photometry of comparison stars in common in the field of SN 2005gj.

Star ID	α (J2000.0)	δ (J2000.0)	<i>u</i>		<i>g</i>		<i>r</i>		<i>i</i>		<i>z</i>	
			SDSS	CSP	SDSS	CSP	SDSS	CSP	SDSS	CSP	SDSS	CSP
1	03 01 09.56	−00 33 52.5	18.639(027)	18.690(054)	17.367(018)	17.362(009)	16.837(022)	16.823(013)	16.643(018)	16.586(010)	16.549(020)	
2	03 01 06.29	−00 32 59.0	19.122(027)	19.043(018)	17.609(014)	17.575(015)	16.191(017)	16.051(017)	15.403(018)	
3	03 01 14.03	−00 31 48.7	19.843(039)	19.899(097)	17.676(016)	17.653(023)	16.745(012)	16.726(015)	16.404(015)	16.362(010)	16.215(017)	
4	03 01 14.44	−00 34 44.3	20.116(026)	20.038(045)	19.579(018)	19.556(062)	19.356(025)	19.113(067)	19.207(040)	
5	03 01 12.99	−00 31 22.5	...	20.262(436)	18.856(021)	18.770(015)	17.345(009)	17.323(009)	16.595(014)	16.505(010)	16.145(064)	
6	03 01 21.27	−00 32 44.3	16.074(030)	16.102(011)	14.556(010)	14.544(011)	13.965(016)	13.961(015)	13.774(007)	13.728(015)	13.711(023)	
7	03 01 07.49	−00 30 51.5	19.915(041)	20.347(285)	18.385(019)	18.384(017)	17.741(020)	17.735(010)	17.502(016)	17.451(013)	17.372(021)	
8	03 01 21.46	−00 34 25.2	18.486(027)	18.533(030)	17.214(011)	17.204(009)	16.694(017)	16.685(009)	16.508(018)	16.473(009)	16.418(016)	
9	03 01 07.16	−00 35 52.2	18.847(021)	18.923(041)	17.458(013)	17.453(009)	16.940(011)	16.936(011)	16.765(018)	16.732(011)	16.679(024)	
10	03 01 12.26	−00 36 14.5	18.285(025)	18.306(026)	16.956(018)	16.935(011)	16.412(011)	16.404(009)	16.208(017)	16.181(009)	16.125(021)	
11	03 01 02.16	−00 35 21.1	20.227(033)	20.118(058)	18.717(014)	18.715(017)	17.861(021)	17.787(014)	17.347(020)	
12	03 01 24.01	−00 34 27.7	18.927(020)	18.860(015)	17.433(014)	17.404(020)	16.669(018)	16.611(010)	16.243(024)	
13	03 01 21.90	−00 35 57.2	18.510(035)	18.529(031)	16.922(017)	16.897(009)	16.249(016)	16.226(011)	15.992(017)	15.958(009)	15.868(016)	
14	03 01 01.95	−00 36 08.2	20.030(065)	20.081(196)	17.833(019)	17.819(010)	16.882(007)	16.864(013)	16.515(017)	16.470(009)	16.306(015)	
15	03 01 26.63	−00 31 51.6	18.748(029)	18.314(545)	16.915(010)	16.888(009)	16.142(013)	16.117(009)	15.845(022)	15.798(009)	15.708(015)	
16	03 01 22.53	−00 30 11.5	18.767(032)	18.834(109)	17.458(013)	17.454(011)	16.896(015)	16.882(009)	16.692(013)	16.652(009)	16.599(018)	

Note. — Uncertainties given in parentheses are in thousandths of a magnitude. For the CSP photometry with the Swope they correspond to the rms of the magnitudes obtained on four photometric nights, with a minimum uncertainty of 0.015 mag for an individual measurement.

Table 2. SDSS and MDM *ugriz* photometry of SN 2005gj

JD −2, 453, 000	Epoch ^a (days)	<i>u</i>	<i>g</i>	<i>r</i>	<i>i</i>	<i>z</i>	Source
616.94	...	24.00±1.24	25.19±0.80	23.81±0.61	23.36±0.54	22.15±0.53	SDSS
626.91	...	21.12±0.70	27.83±0.86	22.85±0.45	24.92±0.93	22.28±1.77	SDSS
628.90	...	23.88±1.45	25.72±1.23	22.92±0.41	25.98±0.45	21.72±0.54	SDSS
635.91	...	22.00±0.49	26.38±1.11	23.32±0.62	23.27±0.59	22.15±0.53	SDSS
639.95	1.9	18.887(045)	18.592(025)	18.621(010)	18.718(016)	18.924(043)	SDSS
641.95	3.8	18.468(034)	18.154(011)	18.256(020)	18.340(016)	18.511(041)	SDSS
644.89	6.6	18.121(023)	17.795(011)	17.879(022)	17.935(010)	18.141(022)	SDSS
656.94	17.9	...	17.355(026)	17.255(029)	17.360(064)	...	MDM
657.90	18.8	17.949(039)	17.343(012)	17.214(012)	17.275(016)	17.438(024)	SDSS
663.89	24.5	18.149(039)	17.410(050)	17.158(012)	17.163(012)	17.280(027)	SDSS
663.92	24.5	...	17.368(025)	17.160(020)	17.248(055)	...	MDM
665.91	26.4	17.146(028)	17.215(054)	...	MDM
666.96	27.3	18.282(043)	17.408(012)	17.121(012)	17.133(013)	17.268(015)	SDSS
668.87	29.2	...	17.393(014)	17.125(026)	17.186(045)	...	MDM
668.88	29.2	18.355(028)	17.401(009)	17.127(012)	17.096(016)	17.240(016)	SDSS
669.97	30.2	18.347(045)	17.430(011)	17.101(014)	17.105(031)	17.231(017)	SDSS
670.88	31.0	18.386(024)	17.419(007)	17.125(013)	17.092(014)	17.249(021)	SDSS
673.85	33.8	18.479(028)	17.450(009)	17.123(012)	17.081(014)	17.229(015)	SDSS
675.85	35.7	18.551(025)	17.477(010)	17.134(029)	17.088(019)	17.182(019)	SDSS
676.90	36.7	...	17.464(043)	17.116(026)	17.138(055)	...	MDM
680.86	40.4	18.663(027)	17.578(009)	17.133(011)	17.054(009)	17.156(016)	SDSS
683.92	43.3	18.759(062)	17.656(034)	17.220(055)	17.080(015)	17.061(066)	SDSS
686.86	46.1	18.887(047)	17.695(014)	17.160(011)	17.060(010)	17.138(021)	SDSS
687.91	47.1	18.937(105)	17.687(013)	17.206(024)	17.042(018)	17.119(026)	SDSS
693.86	52.7	19.018(081)	17.780(009)	17.207(015)	17.084(014)	17.130(018)	SDSS
699.85	58.3	...	17.864(060)	17.271(034)	17.202(057)	17.166(024)	MDM
699.88	58.4	19.083(042)	17.909(013)	17.273(009)	17.124(010)	17.135(020)	SDSS
727.70	84.6	...	18.368(025)	17.639(043)	17.551(053)	17.407(015)	MDM
737.75	94.0	...	18.525(038)	17.791(033)	17.709(063)	17.470(057)	MDM
739.64	95.8	...	18.540(037)	17.822(035)	17.744(065)	17.548(027)	MDM

Note. — Uncertainties given in parentheses in thousandths of a magnitude.

^aRest-frame days since the time of explosion (JD 2,453,637.93).

Table 3. CSP $u'g'r'i'$ photometry of SN 2005gj

JD –2,453,000	Epoch (days)	u'	g'	r'	i'
698.69	57.2	19.159(042)	17.884(017)	17.243(017)	17.106(017)
699.67	58.2	19.196(041)	17.910(017)	17.261(017)	17.100(017)
702.68	61.0	19.286(042)	17.959(017)	17.281(017)	17.130(017)
706.69	64.8	19.312(040)	18.031(017)	17.345(017)	17.173(017)
712.64	70.4	19.619(060)	18.157(017)	17.418(017)	17.249(017)
720.66	77.9	19.721(131)	18.283(023)	17.542(017)	17.363(017)
725.65	82.6	19.964(079)	18.365(017)	17.602(017)	17.412(017)
728.71	85.5	19.938(104)	18.430(017)	17.658(017)	17.453(017)
736.62	93.0	20.104(084)	18.554(017)	17.794(017)	17.586(017)
740.64	96.8	20.229(090)	18.606(017)	17.856(017)	17.641(017)
741.59	97.6	20.238(103)	18.635(017)	17.872(017)	17.651(017)
746.61	102.4	20.532(220)	18.641(025)	17.926(017)	17.725(017)
754.58	109.9	20.509(143)	18.770(017)	18.021(017)	17.803(017)
761.64	116.5	...	18.847(017)	18.100(017)	17.910(018)
763.56	118.3	...	18.841(017)	18.107(017)	17.960(017)
764.58	119.3	...	18.859(017)	18.143(017)	17.947(017)
768.60	123.1	...	18.882(019)	18.200(017)	17.978(021)
773.55	127.7	...	18.884(026)	18.239(019)	18.050(021)
774.56	128.7	...	18.946(031)	18.221(017)	18.079(022)
783.55	137.2	...	19.017(018)	18.322(017)	18.117(021)
786.53	140.0	...	19.015(017)	18.363(017)	18.178(020)
795.55	148.5	...	19.099(019)	18.416(021)	18.227(031)

Note. — Uncertainties given in parentheses in thousandths of a magnitude.

Table 4. CSP $YJHK_s$ photometry of SN 2005gj

JD −2, 453, 000	Epoch (days)	Y	J	H	K_s	Instrument
700.71	59.1	16.565(015)	16.484(034)	16.253(030)	...	Retrocam
704.68	62.9	16.591(015)	16.537(020)	16.315(033)	...	Retrocam
709.66	67.6	16.628(015)	16.550(023)	16.271(029)	...	Retrocam
714.58	72.2	16.673(015)	16.594(020)	16.389(028)	...	Retrocam
718.65	76.0	16.725(016)	16.658(022)	16.364(037)	...	Retrocam
722.62	79.8	16.832(016)	16.725(032)	16.490(017)	16.384(096)	WIRC
724.68	81.7	16.781(016)	16.716(028)	Retrocam
727.69	84.6	16.872(024)	16.757(036)	Retrocam
732.71	89.3	16.920(019)	16.839(025)	Retrocam
750.61	106.1	17.307(016)	17.152(016)	16.812(016)	...	WIRC
755.57	110.8	17.337(024)	17.263(024)	16.891(025)	16.745(039)	PANIC
756.59	111.8	17.428(016)	17.269(016)	16.928(017)	...	WIRC
757.60	112.7	17.423(024)	17.270(024)	16.938(025)	16.807(042)	PANIC
773.57	127.8	17.677(016)	17.476(016)	WIRC
776.54	130.6	17.538(026)	17.399(070)	17.081(068)	...	Retrocam
777.55	131.5	17.648(038)	17.417(056)	17.129(119)	...	Retrocam
782.55	136.2	17.513(039)	17.436(073)	17.072(114)	...	Retrocam
783.55	137.2	17.766(024)	17.586(024)	17.271(025)	17.045(042)	PANIC
785.53	139.0	17.765(025)	17.570(022)	17.192(049)	17.152(177)	WIRC
788.54	141.9	17.869(016)	17.594(016)	17.335(019)	...	WIRC
797.52	150.3	17.855(061)	17.563(118)	17.313(158)	...	Retrocam
800.50	153.1	17.840(041)	Retrocam
808.52	160.7	17.871(058)	17.551(079)	Retrocam
814.49	166.3	17.864(084)	Retrocam

Note. — Uncertainties given in parentheses in thousandths of a magnitude.

Table 5. Light-curve parameters for SN 2005gj

Parameter	Value
Time of explosion ^a	637.93 ± 2.02
Time of u_{max}	651.77 ± 0.48
Time of g_{max}	657.80 ± 1.28
Time of r_{max}	672.49 ± 1.39
Time of i_{max}	684.51 ± 1.00
u_{max}	17.85 ± 0.05
g_{max}	17.35 ± 0.01
r_{max}	17.12 ± 0.01
i_{max}	17.05 ± 0.01
u_{max}^0 ^b	17.11 ± 0.12
g_{max}^0	16.94 ± 0.09
r_{max}^0	16.83 ± 0.07
i_{max}^0	16.89 ± 0.11
$M_{g,max}^0$	-20.21
$E(B - V)_{Gal}$ ^c	0.121 ± 0.019
$A_g(Gal)$	0.45 ± 0.07

^aJD-2,453,000

^bMagnitudes at maximum in the rest-frame, they have been corrected by Galactic extinction and K -corrections. We assume a negligible extinction in the host galaxy.

^cFrom Schlegel et al. (1998)

Table 6. Spectroscopic observations of SN 2005gj

JD −2, 453, 000	Epoch (days)	Instrument	Wavelength Range (Å)	Resolution ^a (Å)	Exposure (s)
644.92	6.6	MDM-CCDS	3850 – 7308	15	1200
646.95	8.5	ARC-DIS	3824 – 10192	7	1800
650.84	12.2	ARC-DIS	3600 – 9597	7	1000
655.87	16.9	MDM-CCDS	3823 – 7283	15	1800
665.92	26.4	MDM-CCDS	3883 – 7341	15	2700
668.83	29.1	MDM-CCDS	3886 – 7346	15	2700
676.79	36.6	MDM-CCDS	3882 – 7338	15	3600
684.73	44.1	WHT-ISIS	3924 – 8901	4	1800
686.79	46.0	MDM-CCDS	3858 – 7315	15	2700
698.67	57.2	duPont-ModSpec	3780 – 7290	7	2700
699.67	58.2	duPont-ModSpec	3780 – 7290	7	2700
700.76	59.2	MDM-CCDS	3933 – 7391	15	2700
702.73	61.1	MDM-CCDS	3856 – 7310	15	2700
712.73	70.5	MDM-CCDS	3831 – 7286	15	2700
722.71	79.9	NTT-EMMI	4000 – 10200	9	2700
724.66	81.7	duPont-WFCCD	3800 – 9235	6	2700
725.65	82.6	duPont-WFCCD	3800 – 9235	6	2700
726.66	83.6	duPont-WFCCD	3800 – 9235	6	3600
727.67	84.5	duPont-WFCCD	3800 – 9235	6	3600
728.67	85.5	duPont-WFCCD	3800 – 9235	6	3600
729.67	86.4	MDM-CCDS	3915 – 7373	15	2700
737.70	94.0	MDM-CCDS	3909 – 7368	15	2700
751.60	107.1	NTT-EMMI	3200 – 10200	9	2700
755.62	110.9	MDM-CCDS	3844 – 7299	15	3600
759.61	114.6	Magellan-LDSS-3	3788 – 9980	3	3600
799.52	152.2	duPont-WFCCD	3800 – 9235	6	1200

Note. — Most of the spectra are the combination of multiple observation, the total exposure is given.

^aAverage resolution obtained from the FWHM of arc-lamp lines.

Table 7. K -corrections of SN 2005gj

Epoch (days)	K_u	K_g	K_r	K_i	K_z
6.6	0.039	-0.077	-0.053	-0.141	-0.133
12.2	0.162	-0.097	-0.005	-0.196	-0.047
16.9	0.226	-0.052	-0.055	-0.135	-0.223
26.4	0.276	-0.015	-0.058	-0.116	-0.228
29.1	0.255	0.008	-0.056	-0.104	-0.239
36.6	0.296	0.034	-0.030	-0.118	-0.096
46.0	0.251	0.063	-0.025	-0.079	-0.201
57.2	0.195	0.106	0.049	-0.123	-0.152
58.2	0.186	0.101	0.013	-0.068	-0.216
59.2	0.313	0.090	0.006	-0.072	-0.215
61.1	0.241	0.091	0.011	-0.096	-0.136
70.5	0.505	0.086	0.055	-0.113	-0.054
79.9	0.439	0.112	0.046	-0.090	-0.115
81.7	0.328	0.118	0.063	-0.096	-0.057
82.6	0.340	0.115	0.063	-0.104	-0.102
83.6	0.378	0.105	0.079	-0.099	-0.101
84.5	0.326	0.104	0.071	-0.104	-0.026
85.5	0.391	0.112	0.078	-0.110	-0.036
86.4	0.330	0.124	0.066	-0.094	-0.071
94.0	0.249	0.126	0.094	-0.081	-0.092
107.1	0.266	0.141	0.082	-0.084	-0.089
110.9	0.337	0.138	0.097	-0.091	-0.007

Table 8. Derived integrated luminosity and black-body fits.

Epoch (days)	$\log L_{(u \rightarrow i)}$ (erg s ⁻¹)	$\log L_{(u \rightarrow z)}$ (erg s ⁻¹)	$\log L_{bol}$ (erg s ⁻¹)	T_{bb}^a (K)	R_{bb}^b (10 ¹⁵ cm)	χ_ν^2 ^c
1.9	42.822	42.862	43.285(0.109)	12898(1193)	1.02(0.16)	0.7
3.8	42.990	43.029	43.485(0.105)	13552(1316)	1.16(0.18)	0.3
6.6	43.141	43.180	43.637(0.098)	13569(1288)	1.38(0.21)	0.2
18.8	43.344	43.389	43.713(0.096)	10955(831)	2.32(0.34)	1.2
24.5	43.335	43.387	43.644(0.125)	9468(612)	2.87(0.42)	1.2
27.3	43.335	43.388	43.628(0.135)	9069(720)	3.06(0.50)	2.2
29.2	43.335	43.389	43.617(0.140)	8772(683)	3.22(0.53)	2.3
30.2	43.334	43.388	43.617(0.137)	8761(692)	3.23(0.54)	2.3
31.0	43.332	43.386	43.611(0.122)	8697(705)	3.25(0.55)	2.6
33.8	43.325	43.381	43.595(0.140)	8392(685)	3.43(0.59)	2.9
35.7	43.316	43.374	43.581(0.160)	8100(582)	3.61(0.59)	2.4
40.4	43.299	43.361	43.559(0.152)	7684(526)	3.92(0.64)	2.5
43.3	43.270	43.338	43.532(0.143)	7284(335)	4.24(0.59)	0.6
46.1	43.269	43.336	43.526(0.101)	7142(477)	4.36(0.73)	2.8
47.1	43.263	43.332	43.523(0.139)	7115(450)	4.38(0.70)	2.1
52.7	43.247	43.317	43.506(0.123)	6889(425)	4.58(0.74)	2.4
57.2	43.219	43.294	43.480(0.095)	6958(247)	4.32(0.54)	2.0
58.2	43.212	43.288	43.473(0.096)	6913(248)	4.34(0.55)	2.0
58.4	43.215	43.290	43.480(0.133)	6656(322)	4.78(0.70)	1.6
61.0	43.198	43.274	43.458(0.107)	6840(261)	4.34(0.56)	2.4
64.8	43.176	43.254	43.438(0.087)	6830(249)	4.27(0.54)	2.2
70.4	43.133	43.214	43.394(0.109)	6570(278)	4.33(0.58)	3.4
77.9	43.088	43.171	43.355(0.098)	6633(280)	4.10(0.54)	2.8
82.6	43.057	43.143	43.321(0.127)	6380(293)	4.18(0.58)	4.2
85.5	43.038	43.125	43.305(0.096)	6459(282)	4.04(0.54)	3.5
93.0	42.987	43.076	43.256(0.103)	6360(272)	3.92(0.53)	3.6
96.8	42.963	43.054	43.232(0.101)	6305(279)	3.87(0.53)	3.9
97.6	42.955	43.047	43.226(0.105)	6318(279)	3.83(0.52)	3.8
102.4	42.935	43.026	43.205(0.133)	6372(332)	3.68(0.52)	4.4
109.9	42.896	42.989	43.165(0.117)	6339(313)	3.53(0.50)	4.4
116.5	42.859	42.953	43.135(0.123)	6549(350)	3.25(0.46)	3.8
118.3	42.855	42.947	43.128(0.138)	6566(362)	3.21(0.46)	4.0
119.3	42.847	42.940	43.122(0.117)	6548(357)	3.20(0.46)	4.0
120.2	42.839	42.932	43.114(0.120)	6536(352)	3.18(0.45)	3.9
123.1	42.831	42.924	43.104(0.127)	6533(370)	3.14(0.45)	4.3
127.7	42.818	42.909	43.087(0.155)	6523(399)	3.06(0.46)	5.0
128.7	42.809	42.901	43.078(0.153)	6486(399)	3.07(0.46)	5.2
137.2	42.776	42.869	43.043(0.169)	6404(418)	2.99(0.46)	6.3
140.0	42.766	42.857	43.030(0.197)	6377(421)	2.96(0.46)	6.5
148.5	42.738	42.830	42.999(0.205)	6246(438)	2.94(0.48)	8.0

^aBlack-body temperature from the fits to the broadband photometry; 1σ uncertainty are given in parenthesis.

^bBlack-body radius from the fits to the broadband photometry; 1σ uncertainty are given in parenthesis and include a 10% uncertainty in the distance to SN 2005gj.

^c χ^2 per degree of freedom of the black-body fits.

Table 9. Library of spectra used in SNID

SN Name	Class	Epochs	Reference
1990N	Ia normal	-14, -13, -8, -7, -6, 0, 4, 8, 15, 18, 39	1
1991T	Ia 91T	-9, -8, -7, -6, -5, -4, -2, -1, 9, 10, 11, 12, 15, 16, 17, 18, 19, 20, 21, 22, 23, 27, 43, 44, 47, 48, 51, 69, 77	2, 3
1991bg	Ia 91bg	1, 3, 16, 18, 25, 32, 33, 46, 54, 85	4
1992A	Ia normal	-5, -1, 3, 5, 6, 7, 9, 11, 16, 17, 24, 28	5
1994I	Ic normal	-6, -4, -3, 0, 1, 2, 21, 22, 23, 24, 26, 30, 36, 38	6
1997ef	Ic broad	-14, -12, -11, -10, -9, -6, -5, -4, 7, 13, 14, 16, 17, 19, 22, 24, 27, 41, 45, 47, 49, 75, 80, 81	7
1998aq	Ia normal	-9, -8, -3, 0, 1, 2, 3, 4, 5, 6, 7, 19, 21, 24, 31, 32, 36, 51, 55, 58, 60, 63, 66, 79, 82, 91, 211, 231, 241	8
1998bu	Ia normal	-3, -2, -1, 9, 10, 11, 12, 13, 14, 28, 29, 30, 31, 32, 33, 34, 35, 36, 37, 38, 39, 40, 41, 42, 43, 44, 57	9
1998bw	Ic broad	-9, -7, -6, -3, -2, -1, 1, 3, 4, 6, 9, 11, 12, 13, 19, 22, 29, 45, 64, 125, 200, 337, 376	10
1999aa	Ia 91T	-11, -7, -3, -1, 5, 6, 14, 19, 25, 28, 33, 49, 47, 51	11
1999ee	Ia normal	-9, -7, -2, 0, 3, 8, 10, 12, 17, 20, 23, 28, 33, 42	12
1999ex	Ic normal	-1, 4, 13	12
1999by	Ia 91bg	-4, -3, -2, -1, 2, 3, 5, 6, 7, 8, 10, 11, 25, 29, 31, 33, 42	13
2002ap	Ic broad	-5, -4, 3, 8, 10, 17, 19	14
2004aw	Ic normal	1, 5, 6, 8, 15, 21, 22, 26, 28, 39, 35, 44, 49, 63, 64, 236, 260, 413	15
2006aj	Ic broad	-6, -5, -4, -3, -2, -1, 0, 2, 3	16

References. — (1) Leibundgut et al. (1991); (2) Jeffery et al. (1992); (3) Schmidt et al. (1994); (4) Leibundgut et al. (1993); (5) Kirshner et al. (1993); (6) Millard et al. (1999); (7) Iwamoto et al. (2000); (8) Branch et al. (2003); (9) Jha et al. (1999); (10) Patat et al. (2001); (11) Garavini et al. (2004); (12) Hamuy et al. (2002); (13) Garnavich et al. (2004); (14) Gal-Yam et al. (2002); (15) Taubenberger et al. (2006); (16) Modjaz et al. (2006).

Table 10. Results of the Gaussian fits to H α and H β features

JD −2, 453, 000	Epoch (days)	H α (narrow)		H α (broad)		H β	
		FWHM ^a (km s ^{−1})	flux ^b (10 ^{−14} erg s ^{−1} cm ^{−2})	FWHM ^a (km s ^{−1})	flux ^b (10 ^{−14} erg s ^{−1} cm ^{−2})	FWHM ^a (km s ^{−1})	flux ^b (10 ^{−14} erg s ^{−1} cm ^{−2})
644.92	6.6	...	0.24(0.02)	1575	0.58(0.06)	776	0.50(0.05)
646.95	8.5	137	0.37(0.04)	1481	0.83(0.08)	1307	0.52(0.06)
650.84	12.2	314	0.69(0.07)	1731	1.25(0.13)	1462	0.75(0.10)
655.87	16.9	...	0.57(0.06)	1555	1.11(0.11)	1339	0.75(0.09)
665.92	26.4	...	0.53(0.05)	1569	1.03(0.10)	523	0.48(0.06)
668.83	29.1	...	0.37(0.04)	1234	0.99(0.10)	1275	0.55(0.07)
676.79	36.6	...	0.45(0.05)	1513	0.77(0.08)	884	0.28(0.04)
686.79	46.0	...	0.41(0.04)	1836	0.71(0.07)	...	0.15(0.02)
698.67	57.2	...	0.45(0.04)	2115	0.91(0.10)	...	0.15(0.03)
699.67	58.2	...	0.34(0.04)	2053	0.76(0.08)	...	0.14(0.03)
700.76	59.2	...	0.36(0.04)	1830	0.77(0.08)	620	0.16(0.02)
702.73	61.0	...	0.41(0.04)	1978	0.67(0.07)	...	0.11(0.02)
712.73	70.5	...	0.41(0.04)	2357	1.02(0.11)	...	0.11(0.02)
722.71	79.9	...	0.34(0.04)	2413	1.03(0.11)	490	0.12(0.03)
724.66	81.7	...	0.34(0.04)	2137	0.99(0.10)	1067	0.19(0.03)
725.65	82.6	...	0.34(0.03)	2260	1.02(0.11)	568	0.11(0.02)
726.66	83.6	...	0.35(0.04)	2322	1.10(0.11)	...	0.08(0.02)
727.67	84.5	160	0.32(0.03)	2364	1.02(0.10)	...	0.10(0.02)
728.67	85.5	...	0.20(0.02)	1802	1.24(0.14)	1127	0.19(0.03)
729.67	86.4	...	0.37(0.04)	2687	1.15(0.12)	680	0.14(0.02)
737.70	94.0	...	0.29(0.03)	1941	0.85(0.09)	459	0.09(0.01)
755.62	110.9	...	0.32(0.03)	2236	1.14(0.12)	1031	0.16(0.02)
799.52	152.2	525	0.51(0.05)	3809	2.18(0.22)	1669	0.23(0.03)

^aFWHM is not presented when the spectral resolution is bigger than the measured value.

^b1 σ uncertainties are given in parentheses.

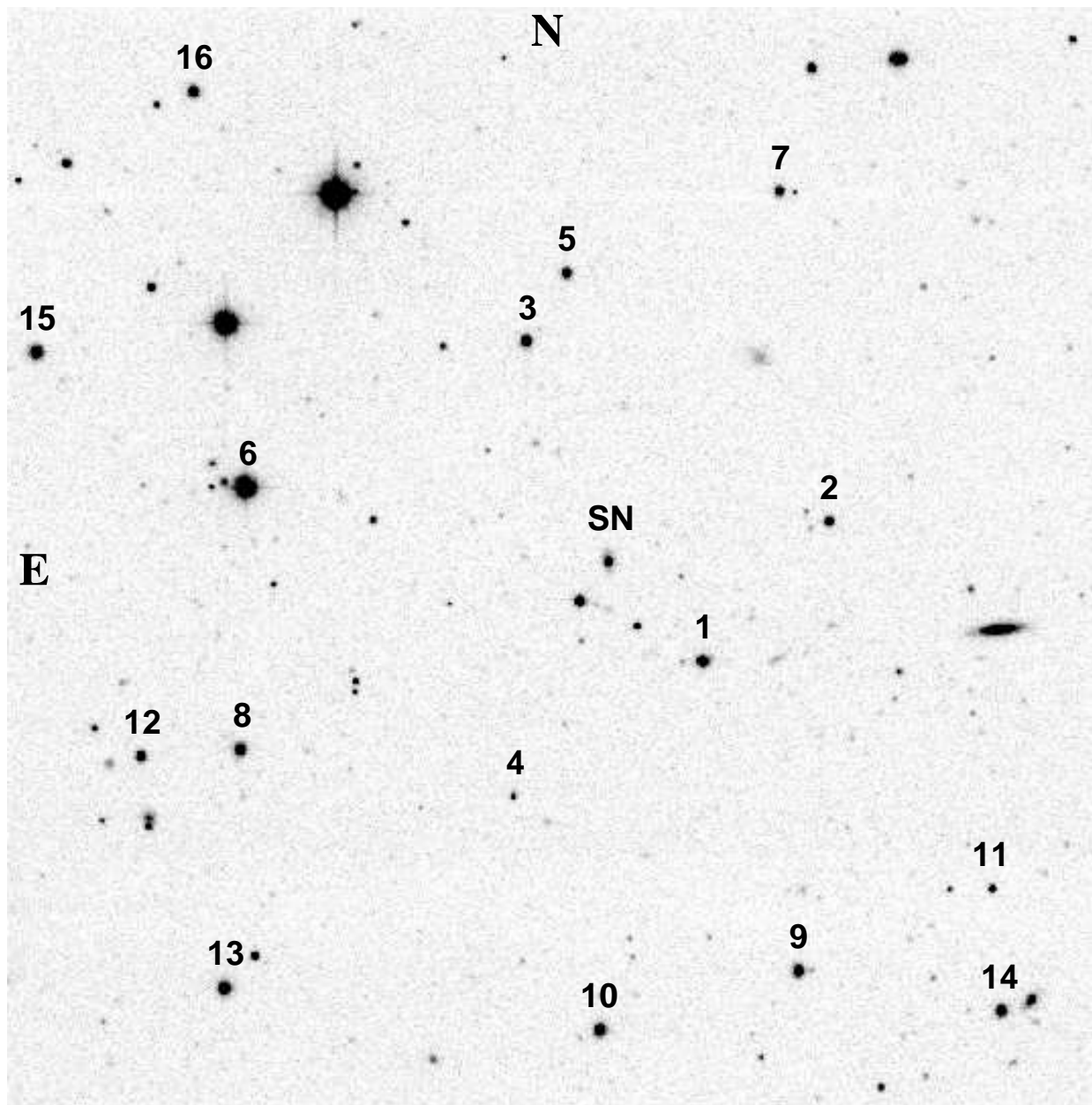


Fig. 1.— r' -band image ($3.5' \times 3.5'$) of the field around SN 2005gj obtained with the Swope-1m telescope at LCO. North is up and east is to the left. Sixteen comparison stars in common between SDSS and CSP used to derive differential photometry of the SN are labeled as in Table 1. The SN is close to the center of the field.

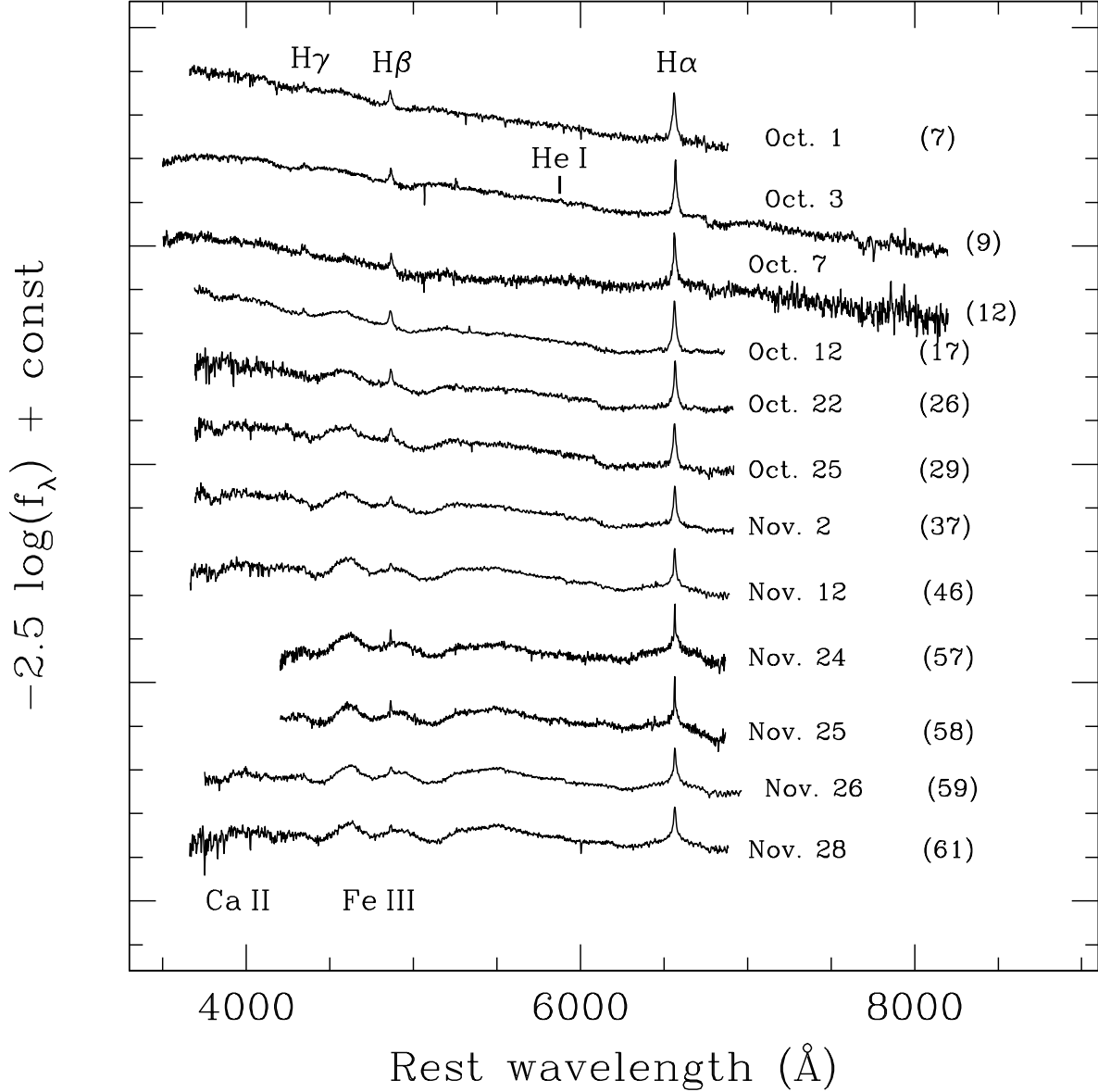


Fig. 2.— Spectra of SN 2005gj obtained from Oct. 1 (~ 7 days after explosion) to Nov. 28 (~ 61 days after explosion) of 2005. The sequence show the dramatic spectral evolution of the SN from a very blue continuum with strong Hydrogen-Balmer lines in emission in the early phases, resembling the spectrum of a Type IIn SN, to a Type Ia supernova-dominated continuum with broad absorption and emission features (P-cygni profiles) of blended Fe II and Fe III profiles. The spectra are shown in logarithmic flux scale and a constant shift has been applied for clarity. The wavelength is in the rest-frame corrected using $z = 0.0616$ for the host galaxy. We show the UT date when the spectra were obtained and the epoch (rest-frame days after explosion) in parenthesis.

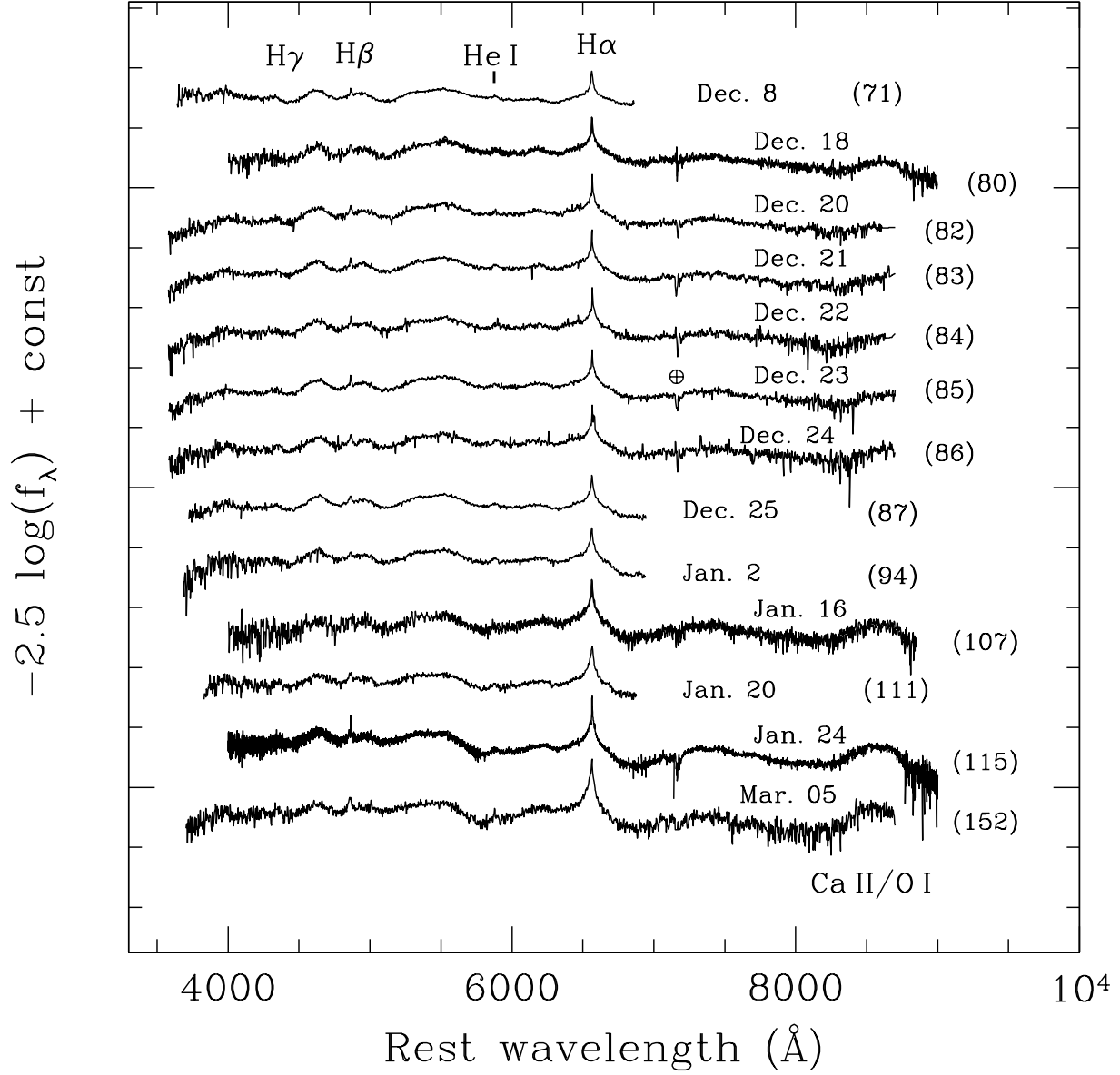


Fig. 3.— Late time spectra of SN 2005gj obtained between Dec. 8, 2005 (~ 71 days after explosion) and Mar. 6, 2006 (~ 152 days after explosion). The labels, axis and symbols are the same as in Figure 2. The *earth* symbol shows the position of a telluric feature present in some of the spectra.

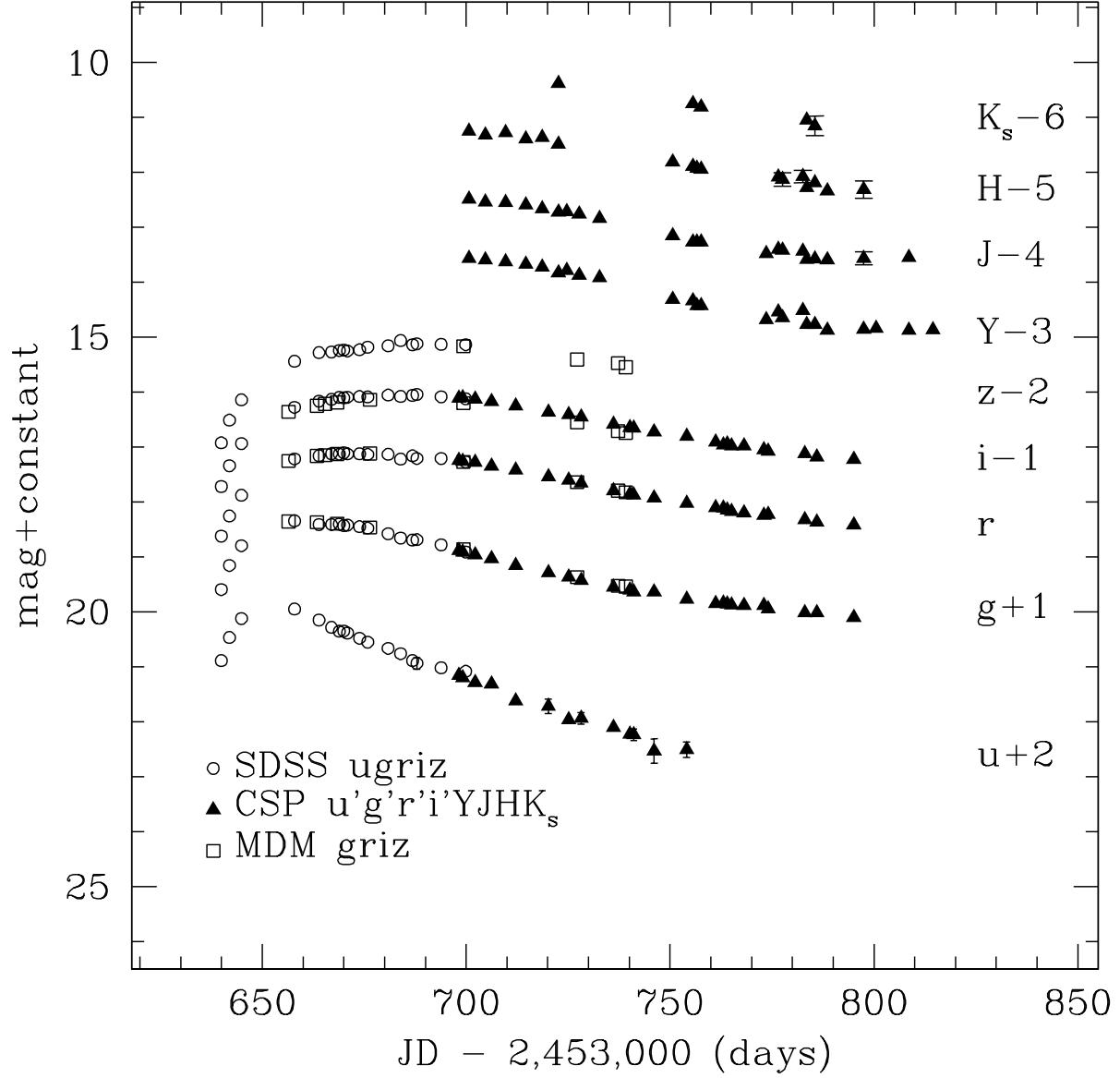


Fig. 4.— Observed light curves of SN 2005gj from SDSS (*open circles*), MDM (*open squares*) and CSP/Swope (*filled triangles*). The error bars are smaller than the symbols. For clarity, the light curves have been shifted by an arbitrary constant.

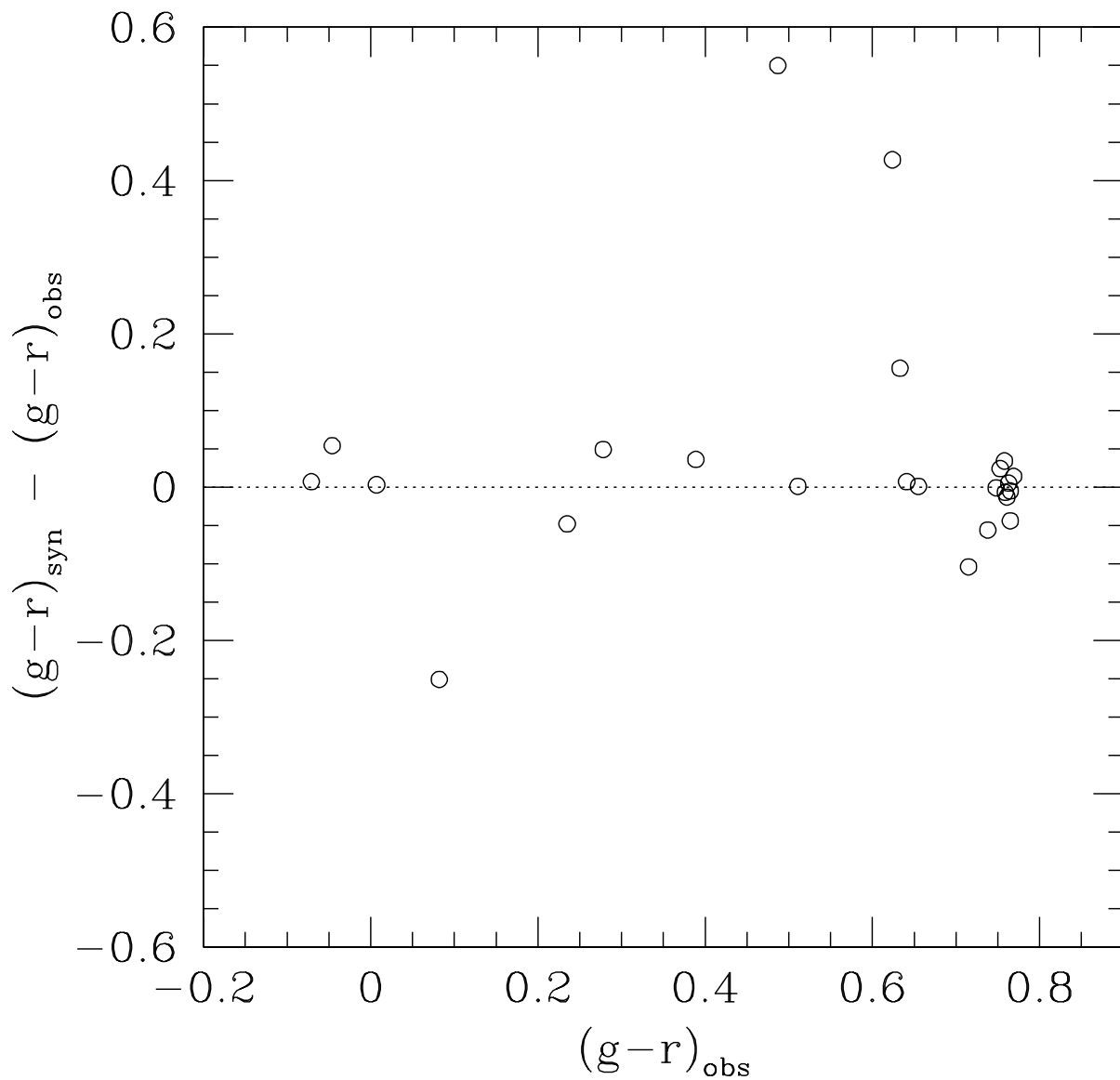


Fig. 5.— Difference between the synthetic $g-r$ color calculated from the spectra and the observed color from the photometry. We do not include the latest spectra obtained on Jan 24. and Mar. 6 because there is no contemporaneous photometric data.

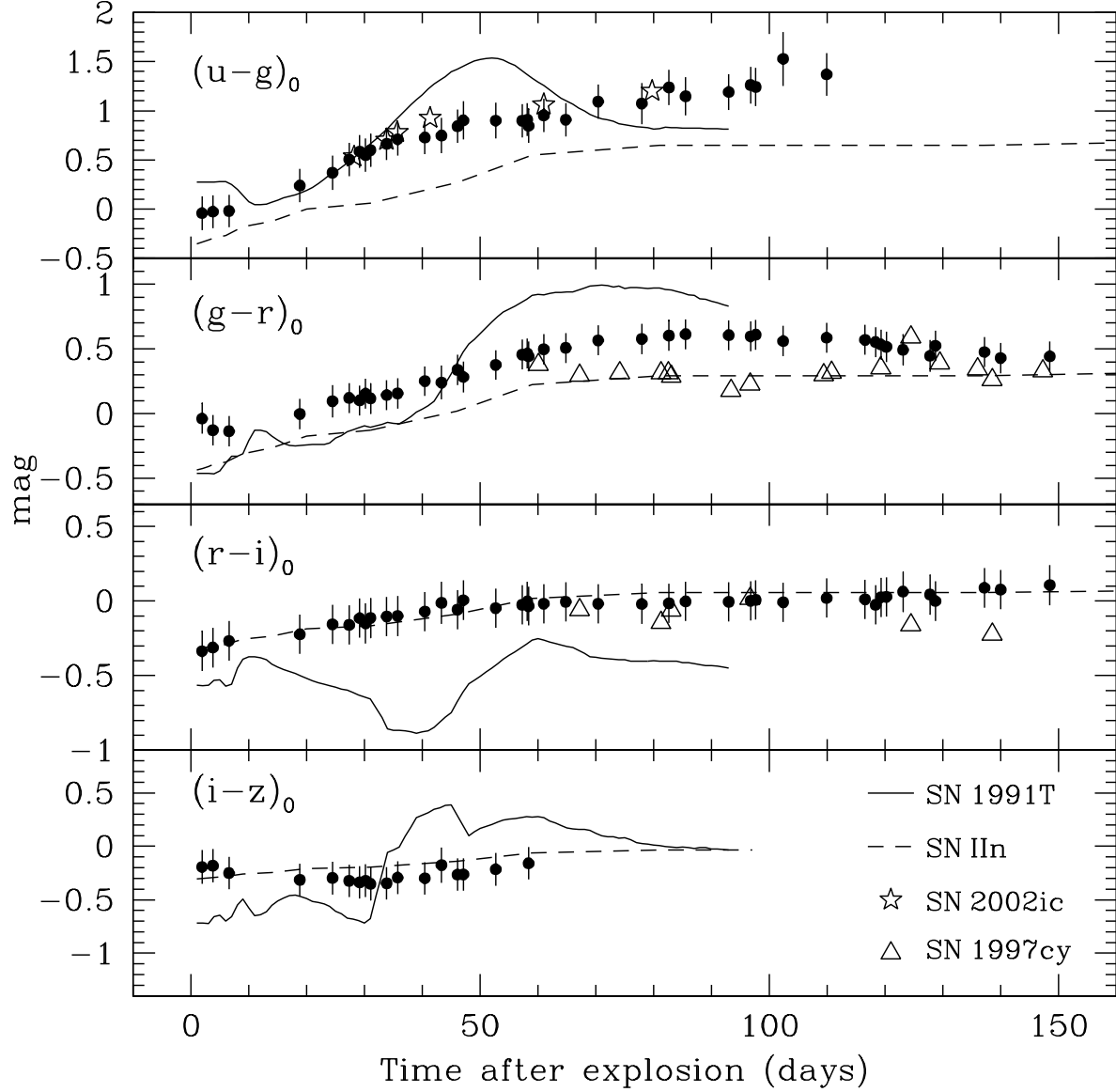


Fig. 6.— Time evolution of the colors of SN 2005gj (*filled circles*). For comparison we also show the color evolution of the overluminous Type Ia SN 1991T (*solid line*), the Type IIn SN 1999el (*dashed line*), and two previous cases of Type Ia strongly interacting with its circumstellar medium, SN 2002ic (*stars*) and SN 1997cy (*triangles*).

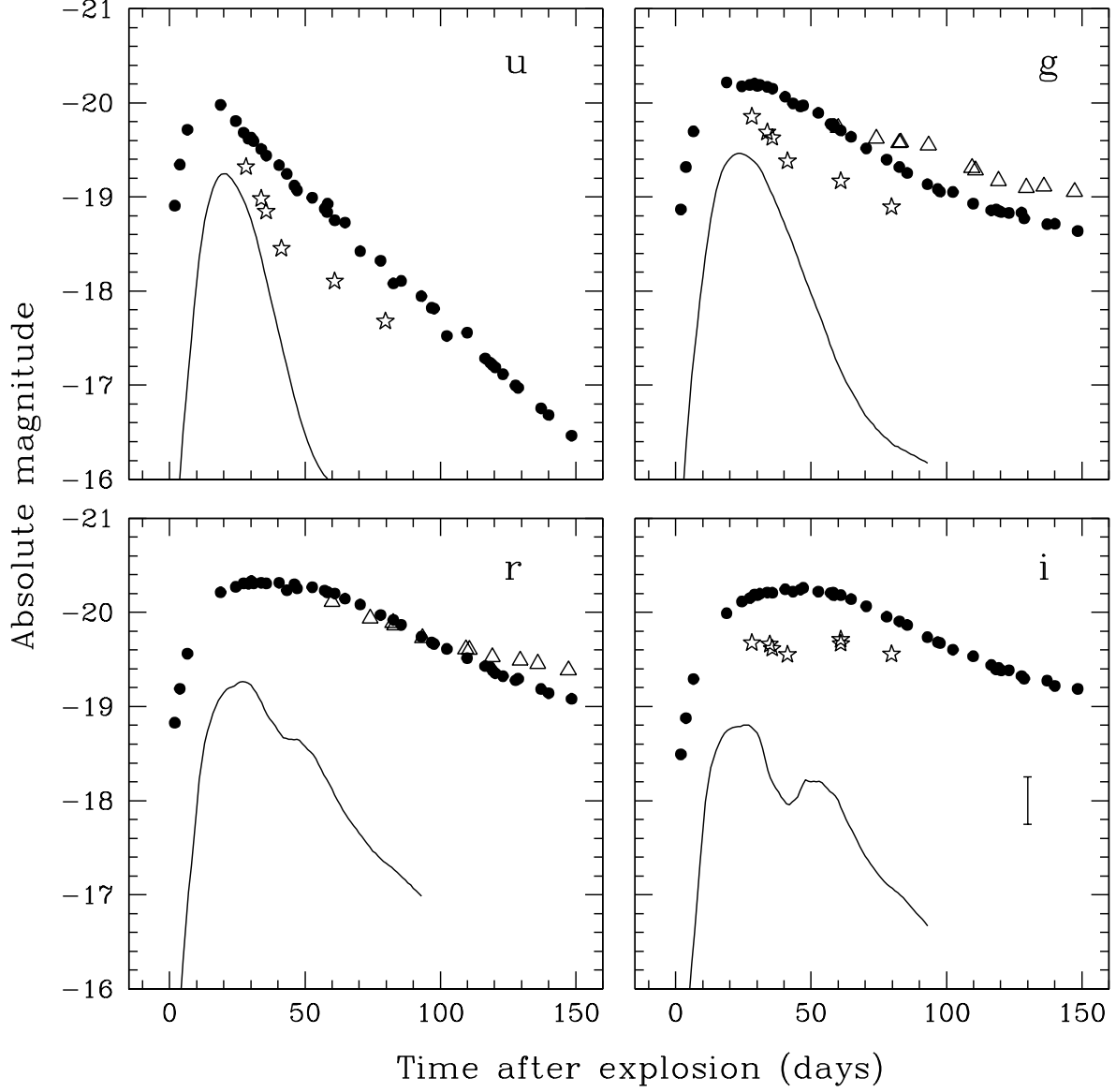


Fig. 7.— Absolute *ugri* light curves of SN 2005gj (*filled circles*). For comparison we also show the absolute light curves of the overluminous Type Ia SN 1991T (*solid line*), SN 2002ic (*stars*) and SN 1997cy (*triangles*). The error bar in the lower right panel represents the typical error in the absolute magnitudes dominated by a 10% uncertainty in the Hubble constant.

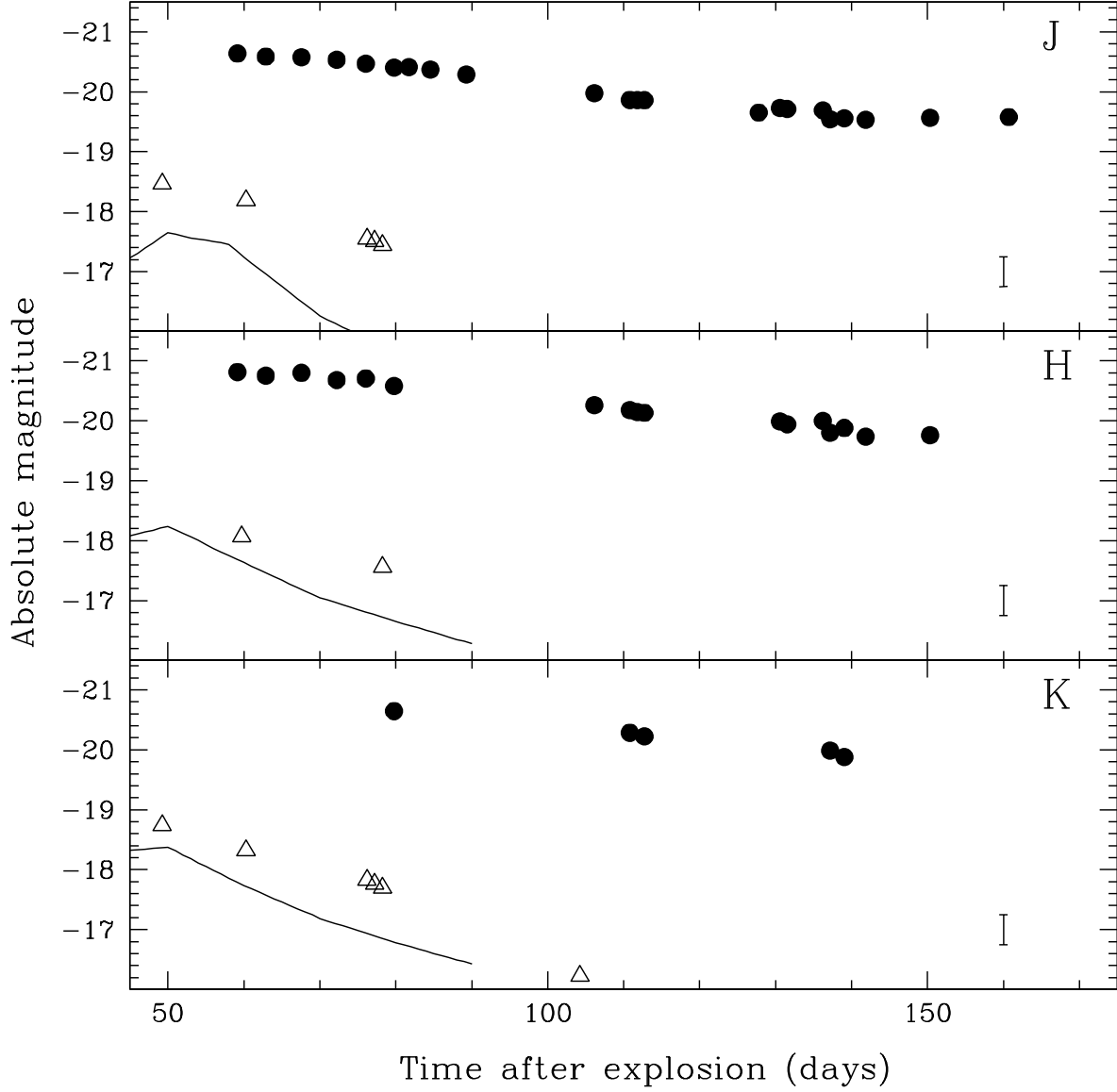


Fig. 8.— Absolute light curves of SN 2005gj in the NIR: *J* (top panel), *H* (middle panel) and *K_s* (bottom panel). For comparison we also show the absolute light curves of a normal Type Ia (solid line) and the Type IIn SN 1999el (open triangles). The error bar in the lower right of each panel represents the typical error in the absolute magnitudes dominated by a 10% uncertainty in the Hubble constant.

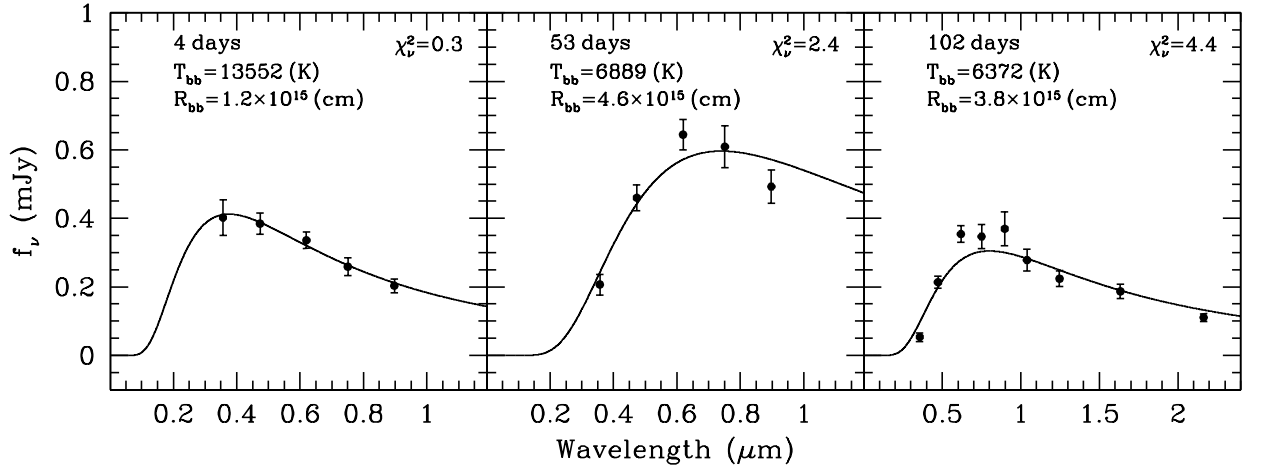


Fig. 9.— Examples of black-body fits (*solid line*) to the SED of SN 2005gj obtained by transforming the rest-frame *ugriz* magnitudes to monochromatic fluxes at the effective wavelength of the filters (*filled circles*). These examples show the quality (i.e., goodness-of-fit) range of the black body fits at different epochs: $\chi^2_\nu = 0.3$ (*left panel*), 2.4 (*middle*), 4.4 (*right*). The units of flux density in the y-axis are $\text{mJy} = 10^{-26} \text{ erg s}^{-1} \text{ cm}^{-2} \text{ Hz}^{-1}$.

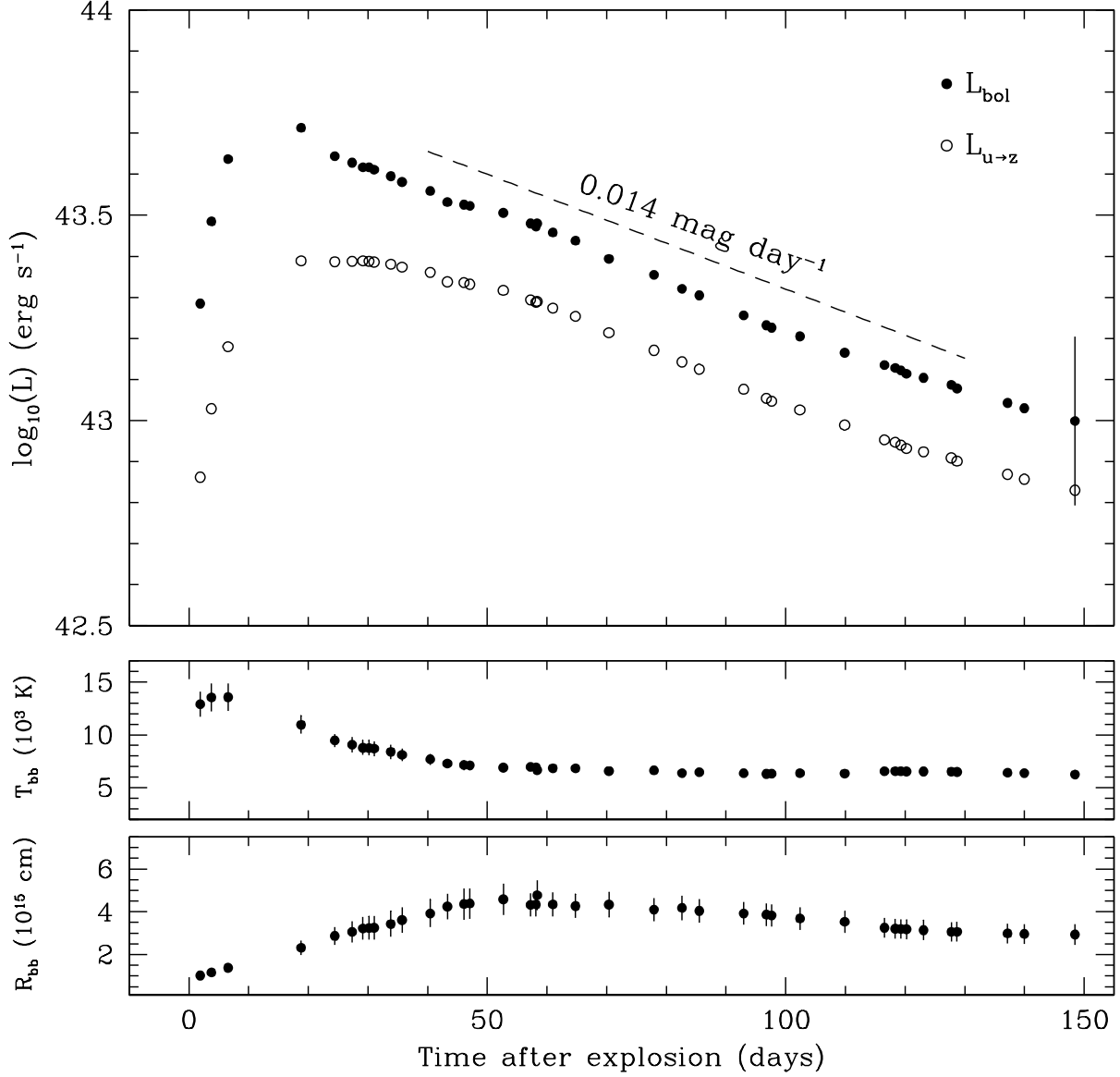


Fig. 10.— *Top panel:* Quasi-bolometric (*open circles*) and bolometric light curves of SN 2005gj (*filled circles*). The bolometric light luminosities were obtained after applying bolometric corrections calculated from black-body fits to the optical SED obtained from the *ugriz* photometry. The *dashed* line shows the best-fit linear decay of $0.014 \text{ mag day}^{-1}$. The *middle* and *bottom panels* show the evolution of the black-body temperature and radius, respectively.

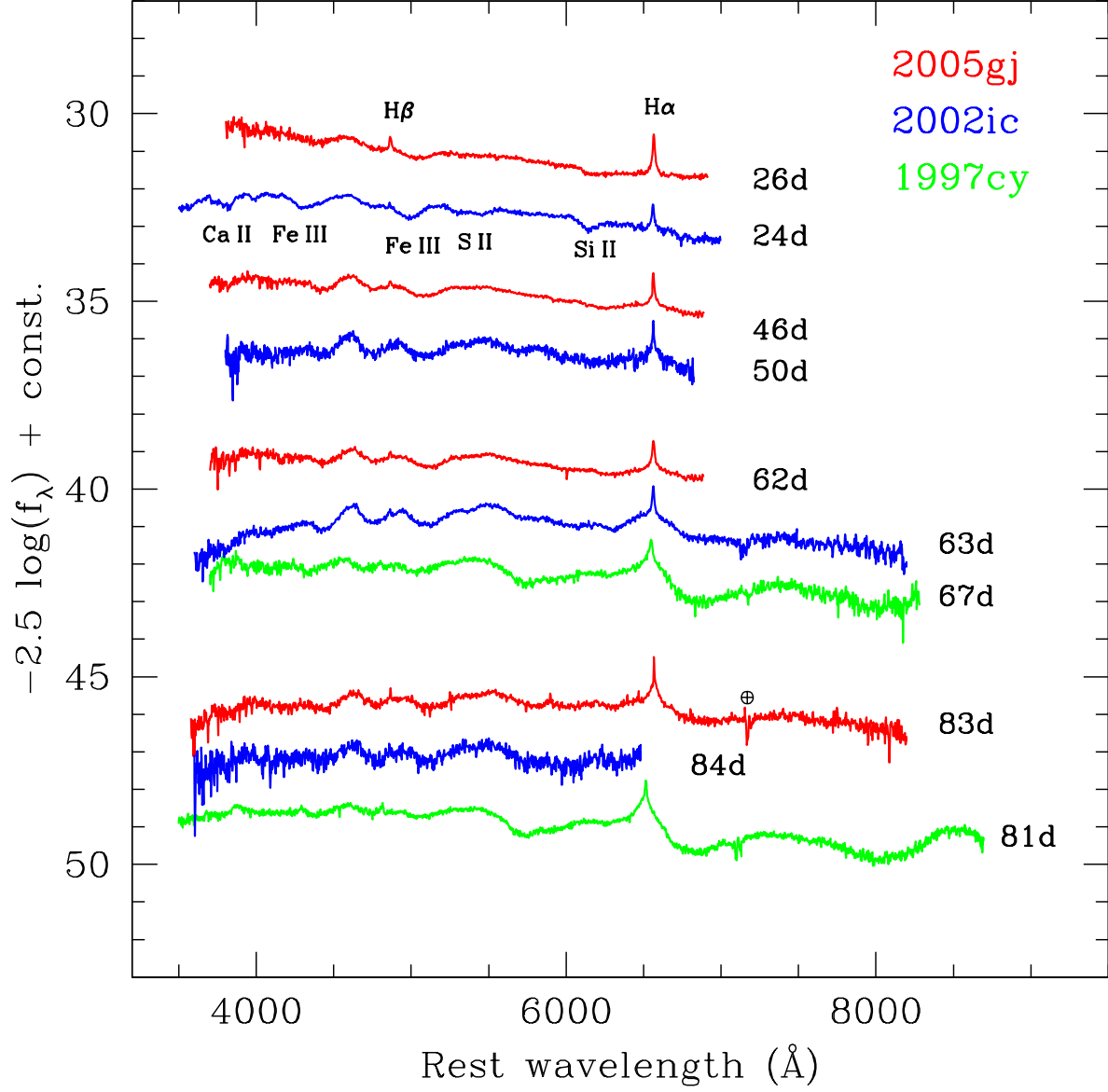


Fig. 11.— Comparison of spectra of SN 2005gj at 26, 46, 62 and 83 days after explosion with comparable epoch spectra of SN 2002ic (Hamuy et al. 2003) and SN 1997cy (from SUSPECT database). The spectra are plotted on a logarithmic flux scale and shifted by an arbitrary constant. The wavelength was shifted to the restframe using $z = 0.0616$ of the host galaxy (Aldering et al. 2006).

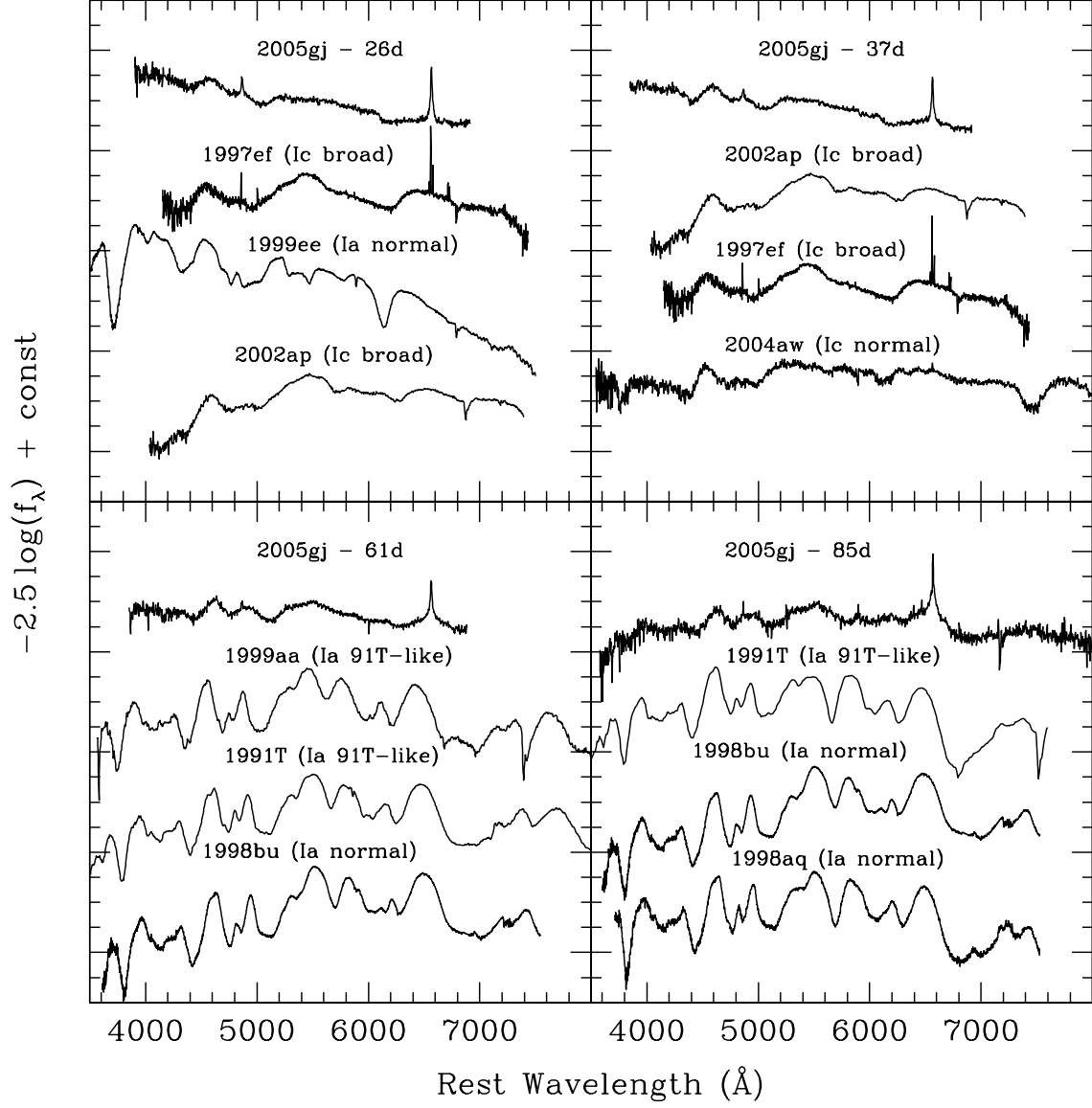


Fig. 12.— Results of SNID. We show the spectra of SN 2005gj at four epochs (26, 37, 61, and 85 days after explosion) and their best three cross-correlation library spectra. The spectra are plotted on a logarithmic flux scale and shifted by an arbitrary constant.

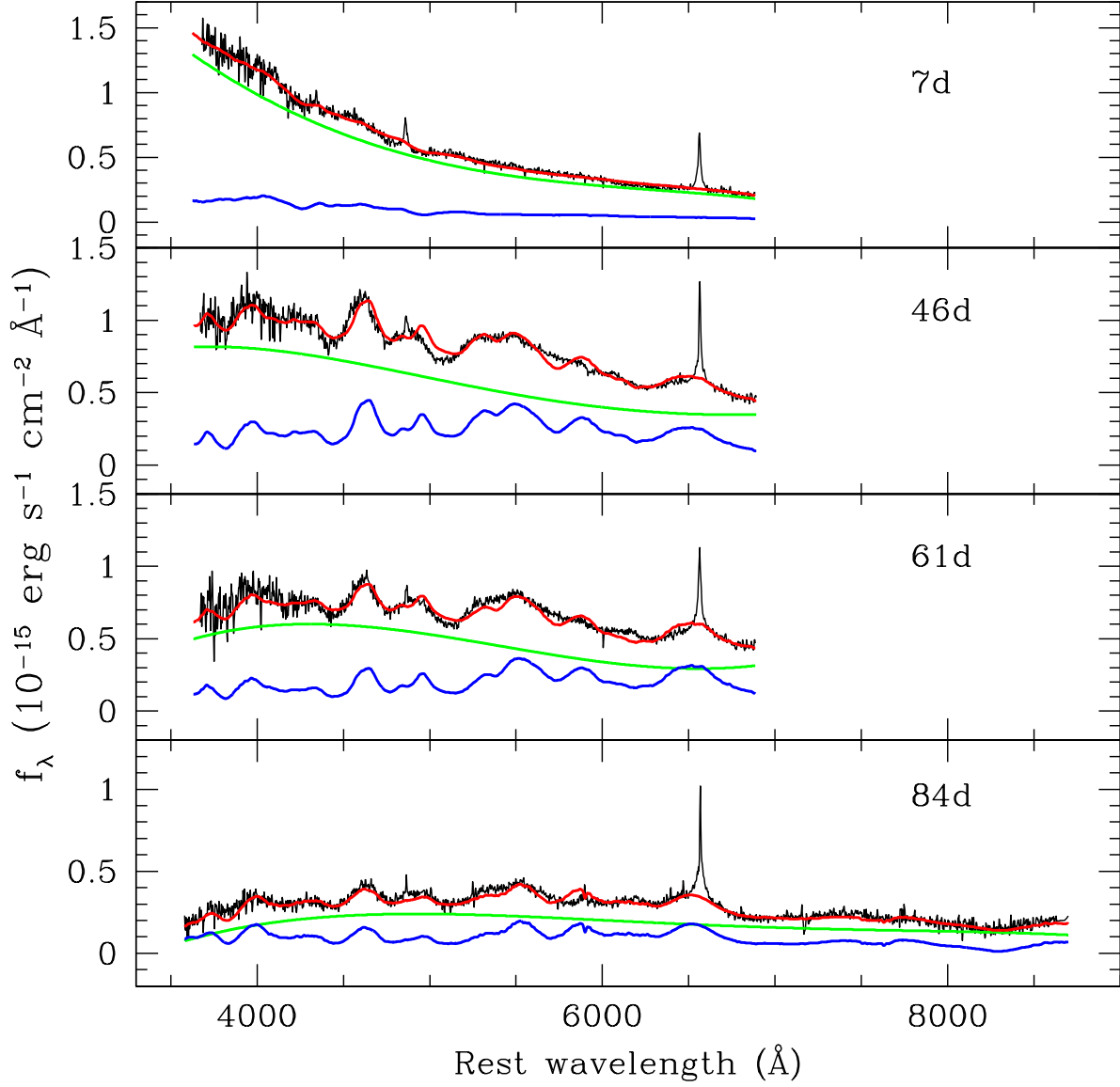


Fig. 13.— Fits to the spectra of SN 2005gj. We model the spectra as the sum of two components: (1) SN 1991T spectrum at the same epoch after explosion as SN 2005gj scaled by an arbitrary constant (*blue line*); (2) fourth order polynomial (*green line*). The results of the fits are in *red* and the spectra of SN 2005gj, corrected by Galactic extinction in the line of sight are in *black*. The epochs of the spectra are shown in the upper right of each panel.

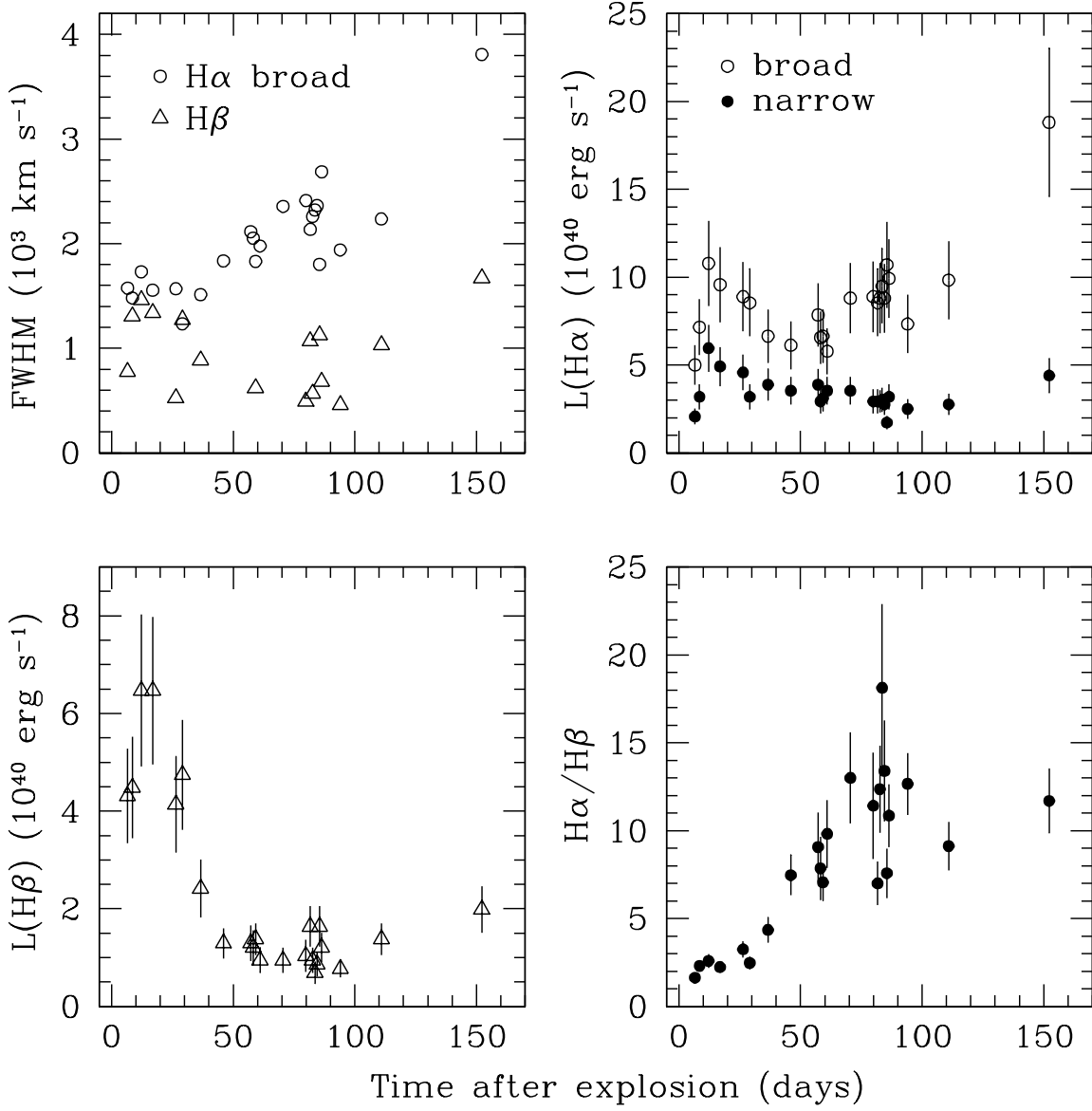


Fig. 14.— Results from the Gaussian fits to H α and H β emission features as a function of time. *Top left panel:* FWHM of the H α -broad and H β . *Top right panel:* Luminosity of the narrow and broad Gaussian components of H α . *Bottom left panel:* Luminosity of H β . *Bottom right panel:* Balmer decrement, ratio of total fluxes in H α and H β lines.

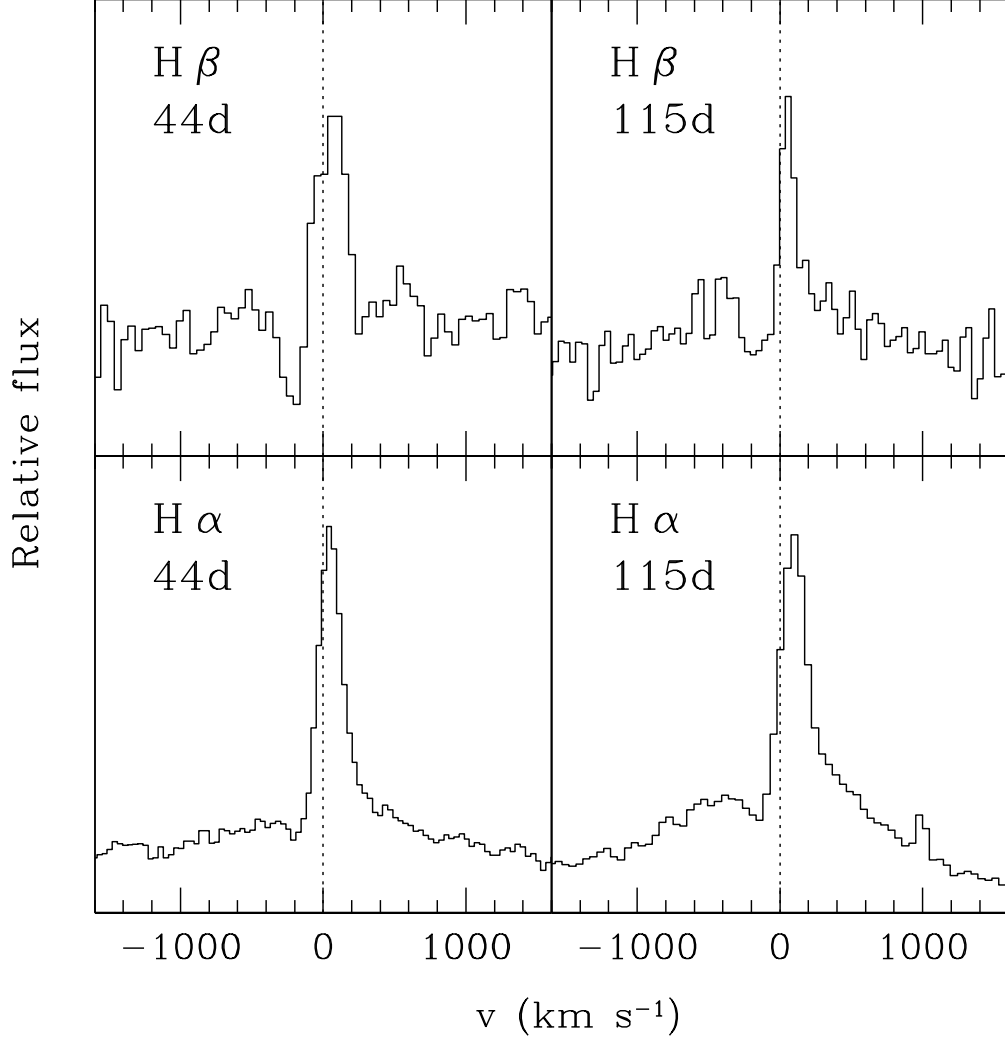


Fig. 15.— Line profiles of H β (*top*) and H α (*bottom*) in the two highest resolution spectra of SN 2005gj obtained with WHT+ISIS on day 44 (*left*) and Magellan+LDSS-3 on day 115 (*right*). The features show clear P-cygni profiles with weak absorption minima at ~ -200 km s⁻¹, demonstrating the presence of a slowly moving outflow.

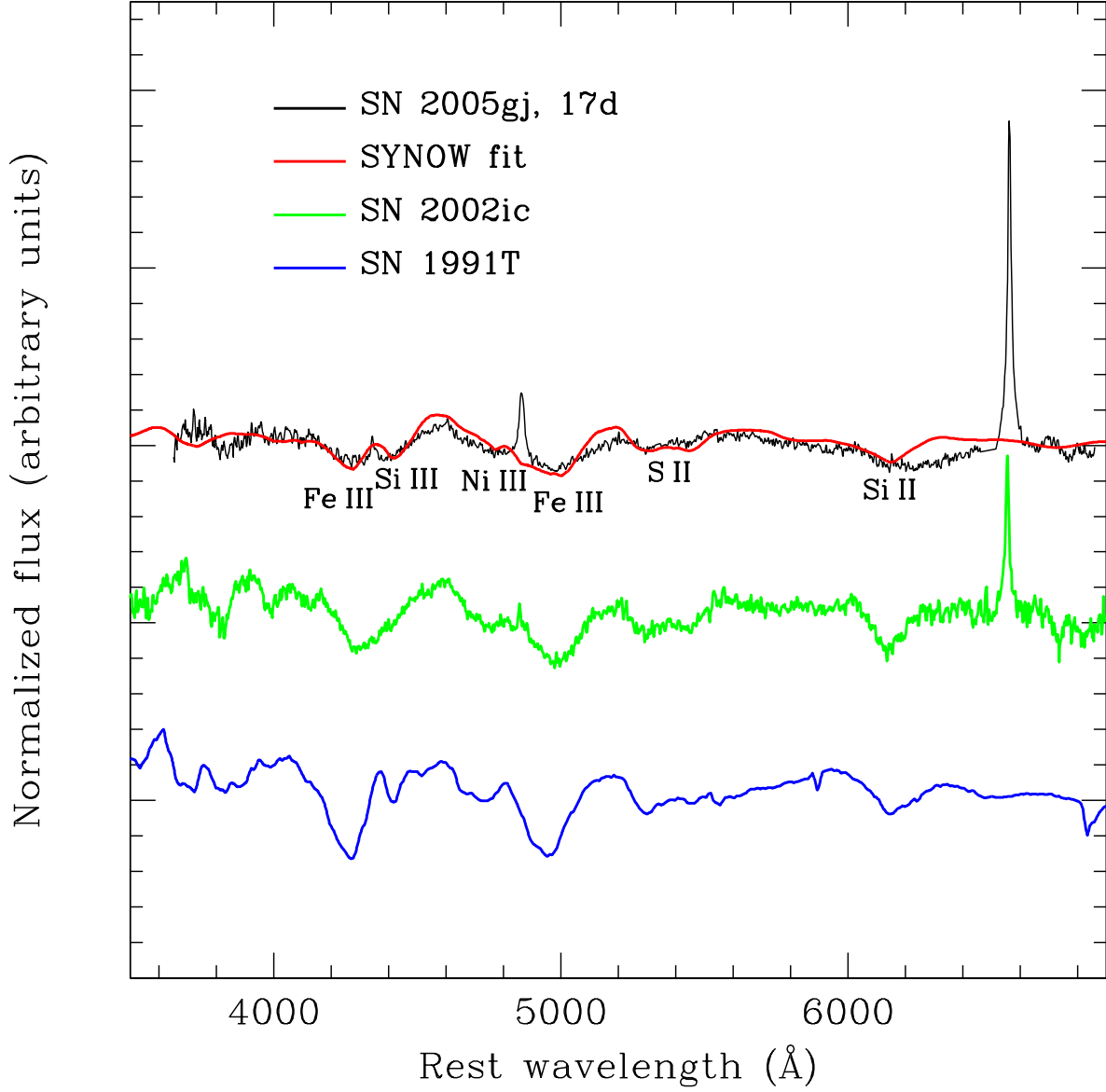


Fig. 16.— Identification of lines in the spectrum of SN 2005gj obtained at 17 days after explosion (2 days before g maximum). The *red line* shows the best fit synthetic spectrum generated with the SYNOW code. The lines of SN 2005gj are typical of SN 1991T around maximum light (*blue line*), and very similar to the spectrum of SN 2002ic around maximum (*green line*). All the spectra have been locally normalized. We have subtracted a constant value to the spectra of SN 2002ic and SN 1991T for clarity.